

Numerical Implementation of the Improved Sugama Collision Operator Using a Moment Approach

B. J. Frei,¹ S. Ernst,¹ and P. Ricci¹

*Ecole Polytechnique Fédérale de Lausanne (EPFL), Swiss Plasma Center,
CH-1015*

(*Electronic mail: baptiste.frei@epfl.ch)

(Dated: 13 March 2022)

The numerical implementation of the linearized gyrokinetic (GK) and drift-kinetic (DK) improved Sugama (IS) collision operators, recently introduced by Sugama *et al.* [Phys. Plasmas **26**, 102108 (2019)], is reported. The IS collision operator extends the validity of the widely-used original Sugama (OS) operator [Sugama *et. al.*, Phys. Plasmas **16**, 112503 (2009)] to the Pfirsch-Schlüter collisionality regime. Using a Hermite-Laguerre velocity-space decomposition of the perturbed gyrocenter distribution function that we refer to as the gyro-moment approach, the IS collision operator is written in a form of algebraic coefficients that depend on the mass and temperature ratios of the colliding species and perpendicular wavenumber. A comparison between the IS, OS, and Coulomb collision operators is performed, showing that the IS collision operator is able to approximate the Coulomb collision operator in the case of trapped electron mode (TEM) in H-mode pedestal conditions better than the OS operator. In addition, the IS operator leads to a level of zonal flow (ZF) residual which has an intermediate value between the Coulomb and the OS collision operators.

I. INTRODUCTION

While the core of fusion devices such as tokamaks and stellarators is sufficiently hot that plasma collisional processes can be neglected, the lower temperature in the boundary region enhances the role of collisions, calling for their accurate description. In fact, while the turbulent particle and heat transport in fusion devices is primarily anomalous, that is driven by small scale electromagnetic instabilities, collisions between particles can still play a crucial role since they may significantly affect the linear properties of these instabilities^{1–3}, their saturation mechanisms via zonal flow generation^{4,5} and the velocity-space structures of the particle distribution functions. In addition, collisions drive the neoclassical processes when turbulent transport is suppressed⁶. An accurate description of collisions might be also important in the transport of heavy impurities, even in the core region because of their large atomic number.

The relatively large value of the Coulomb logarithm ($\ln \Lambda \gtrsim 10$) in fusion devices, where small-angle deflections dominate, allows for the use of the Fokker-Planck collision operator⁷ to describe binary Coulomb collisions between particles. In this work, we refer to the Fokker-Planck collision operator as the Coulomb collision operator. The integro-differential nature of the Coulomb collision operator makes its analytical and numerical treatment challenging. Hence, for practical applications, it is usually assumed that the distribution function is close to a Maxwellian allowing for the linearization of the Coulomb collision operator up to first order in the perturbed quantities. However, the implementation of the linearized Coulomb collision operator remains also challenging. For this reason, approximated linearized collision operator models have been proposed in the literature^{8–11}.

One of the most widely used collision operator models, which we refer to as the linearized original Sugama (OS) collision operator in this work, is originally derived in Ref. 12. The OS collision operator is constructed from the linearized Coulomb collision operator to fulfill the conservation laws (particle, momentum and energy), the entropy production criterion and the self-adjoint relations for arbitrary mass and temperatures ratios of the colliding species. This operator extends previous models¹⁰ to the case of colliding species with different temperatures. While the OS operator is implemented in numerous GK codes and tested in neoclassical and turbulent studies^{13,14}, its deviation with respect to the Coulomb operator is expected to be enhanced when applied in the boundary plasma conditions. For instance, the OS produces a stronger collisional zonal flow damping^{5,15} and can therefore yield turbulent transport levels that can significantly differ from the

Implementation of the Improved Sugama Collision Operator

ones obtained by the Coulomb collision operator¹⁵. A previous study of the collisional effects of ITG reports that the OS Sugama predicts a smaller ITG growth rate at perpendicular wavelength of the order of the ion gyroscale than the Coulomb collision operator¹⁶. Additionally, previous collisional simulations of ZF demonstrate that the OS operator yields a stronger ZF damping than the Coulomb operator in both banana and Pfirsch-Schlüter regime^{5,15}.

To simulate high collisional plasmas while still avoiding the use the Coulomb collision operator, Ref. 17 recently reported on the development of an operator that we refer to as the improved Sugama (IS) collision operator. The IS operator is designed to reproduce the same friction-flow relations (that we define below) of the linearized Coulomb collision operator by adding a correction term to the OS^{18,19}. While the IS operator has been successfully tested and implemented recently in neoclassical simulations using the GT5D code²⁰ where like-species collisions are considered, no direct comparison between the IS, OS and Coulomb collision operators have been reported yet on, e.g., microinstabilities and collisional zonal flow damping.

In this paper, we take advantage of recent analytical and numerical progress made in the development of GK collision operators in Ref. 5 based on a Hermite-Laguerre expansion of the perturbed distribution function²¹, and present the derivation and the expansion of the GK and DK IS collision operators on the same basis. Using the Hermite-Laguerre approach, which we refer to as the gyro-moment approach, the integro-differential nature of collision operator model is reduced to the evaluation of closed analytical expressions involving numerical coefficients that depend on the mass and temperature ratios of the colliding species and, when finite Larmor radius (FLR) terms are included, on the perpendicular wavenumber. By extending Ref. 5, where the linearized GK Coulomb²² and the GK OS collision operators are expanded on the Hermite-Laguerre basis (with the GK OS benchmarked successfully with the GENE code²³), the gyro-moment expansion of the IS collision is derived in the present work. The numerical implementation of the IS collision operator allows us to perform its comparison with the OS as well as the Coulomb collision operators on the study of instabilities and ZF damping for the first time. In particular, the linear properties of the trapped electron modes (TEMs) at steep pressure gradients are investigated and reveal that, indeed, the IS can approach better the Coulomb operator in the Pfirsch-Schlüter regime than the OS operator. Also, all operators yield results that agree within 15% at least for the parameters explored in this work. Nevertheless, larger deviations are expected in the case of heavy impurities²⁴ with temperatures of the colliding species that can be significantly different. Additionally, we show that the IS yields a ZF damping intermediate between the OS and Coulomb

Implementation of the Improved Sugama Collision Operator

collision operators in the Pfirsch-Schlüter regime. Finally, we explicitly evaluate the lowest-order gyro-moment of the IS, OS and Coulomb collision operators that can be used to model collisional effects in reduced gyro-moment models valid under the high-collisionality assumption.

The remainder of the present paper is organised as follows. In Sec. II, the IS collision operator is introduced. Then, in Sec. III, we derive the spherical harmonic expansion of the IS collision operator that allows us to evaluate the GK and DK limits of the same operator. In Sec. IV, we derive closed analytical expressions of the Braginskii matrices of the Coulomb and OS collision operators necessary for the evaluation of the correction terms added to the OS operator. Then, the gyro-moment method is detailed in Sec. V where the Hermite-Laguerre expansion of the GK and DK IS collision operators are obtained analytically. In Sec. VI, numerical tests and comparisons are performed focusing on the TEM at steep pressure gradients and on the study of the collisional ZF damping in the Pfirsch-Schlüter regime. We conclude by discussing the results and future applications in Sec. VII. Appendix A reports on the analytical expressions of the lowest-order gyro-moments of the Coulomb, OS, and IS collision operators, which are useful to derive reduced gyro-moment model for high collisional plasmas.

II. IMPROVED SUGAMA COLLISION OPERATOR

We start by presenting the linearized IS collision operator following the notation and definitions of Ref. 17. We assume that the particle distribution function is perturbed with respect to a Maxwellian distribution of the particle of species a , $f_{Ma} = f_{Ma}(\mathbf{r}, \mathbf{v}) = n_a(\mathbf{r})/\pi^{3/2} v_{Ta}(\mathbf{r})^{3/2} e^{-v^2/v_{Ta}(\mathbf{r})^2}$, with $n_a(\mathbf{r})$ the particle density, $v_{Ta}(\mathbf{r})^2 = 2T_a(\mathbf{r})/m_a$ the thermal particle velocity and $\mathbf{z} = (\mathbf{r}, \mathbf{v})$ the particle phase-space coordinates, being \mathbf{r} the particle position and \mathbf{v} the particle velocity such that $v^2 = \mathbf{v} \cdot \mathbf{v}$. The small-amplitude perturbation, $f_a = f_a(\mathbf{r}, \mathbf{v})$, i.e. $f_a/f_{Ma} \ll 1$, allows us to describe the collisions between species a and b by linearizing a nonlinear collision operator model $C_{ab}^{NL}(f_a, f_b)$. The linearized operator is denoted by $C_{ab} = C_{ab}(\mathbf{r}, \mathbf{v}) = C_{ab}(f_a, f_b)$ and can be written as

$$C_{ab}(f_a, f_b) = C_{ab}^T(f_a) + C_{ab}^F(f_b), \quad (1)$$

where $C_{ab}^T(f_a)$ and $C_{ab}^F(f_b)$ are the test and field components of $C_{ab}(f_a, f_b)$, and are defined from the nonlinear collision operator model, as $C_{ab}^T(f_a) = C_{ab}^{NL}(f_a, f_{Mb})$ and $C_{ab}^F(f_b) = C_{ab}^{NL}(f_{Ma}, f_b)$.

Implementation of the Improved Sugama Collision Operator

Because the test and field components of the Coulomb collision operator involve complex velocity-space derivatives of f_a (e.g. in C_{ab}^T) and integrals f_b (e.g. in C_{ab}^F), approximated linearized collision operators have been proposed for implementation in numerical codes and analytical purposes in the past years^{8,10,12}. Among these simplified models, the OS collision operator model¹², that we denote as C_{ab}^S , is widely used in present GK codes. The C_{ab}^S operator is derived from the linearized Coulomb collision operator, which we denote as C_{ab}^L , to conserve the three lowest-order velocity moments of C_{ab} , i.e.

$$\int d\mathbf{v} C_{ab}(f_a, f_b) = 0, \quad (2a)$$

$$m_a \int d\mathbf{v} \mathbf{v} C_{ab}^T(f_a) = -m_b \int d\mathbf{v} \mathbf{v} C_{ba}^F(f_a), \quad (2b)$$

$$m_a \int d\mathbf{v} v^2 C_{ab}^T(f_a) = -m_b \int d\mathbf{v} v^2 C_{ba}^F(f_a), \quad (2c)$$

and satisfy the H-theorem and the adjointess relations even in the case of collisions between particles with temperatures $T_a \neq T_b$, given by

$$T_a \int d\mathbf{v} \frac{f_a}{f_{Ma}} C_{ab}(f_a, f_b) + T_b \int d\mathbf{v} \frac{f_b}{f_{Mb}} C_{ba}(f_b, f_a) \leq 0, \quad (3)$$

and

$$\int d\mathbf{v} \frac{f_a}{f_{Ma}} C_{ab}^T(g_a) = \int d\mathbf{v} \frac{g_a}{f_{Ma}} C_{ab}^T(f_a), \quad (4a)$$

$$T_a \int d\mathbf{v} \frac{f_a}{f_{Ma}} C_{ab}^F(g_b) = T_b \int d\mathbf{v} \frac{g_b}{f_{Mb}} C_{ba}^F(f_a), \quad (4b)$$

respectively, where f_a and g_a are two arbitrary phase-space (\mathbf{r}, \mathbf{v}) functions. The definitions of the test and field components of C_{ab}^S and C_{ab}^L can be found in Ref. 5 and the analytical derivation of C_{ab}^S in Ref. 12.

The difference between the OS and the Coulomb collision operators is expected to have a larger impact as the collisionality increases, in particular, in the case of particles with different mass and temperature¹. Hence, Ref. 17 proposes to improve the OS collision operator, C_{ab}^S , by adding a correction term, thus defining a new improved operator, that we refer to as the IS collision operator. The IS operator is designed such that it yields to same friction-flow relations¹⁸

Implementation of the Improved Sugama Collision Operator

$$\mathbf{F}_{ai} = (-1)^{i-1} \int d\mathbf{v} m_a \mathbf{v} L_{i-1}^{3/2}(s_a^2) \sum_b C_{ab}(f_a, f_b), \quad (5)$$

than the Coulomb collision operator. In Eq. (5), $s_a^2 = v^2/v_{Ta}^2$ is the energy coordinate and $L_i^{3/2}(x)$ (with $i = 0, 1, 2, \dots$) is the associated Laguerre polynomial defined by

$$L_i^{p+1/2}(x) = \sum_{l=0}^i L_{il}^p x^l, \quad (6)$$

with $L_{il}^p = (-1)^l (p+i+1/2)! / [(i-l)!(l+p+1/2)!l!]$. The derivation of the correction term added to C_{ab}^S can be found in Ref. 17 and we report the results here.

The linearized IS collision operator, denoted by C_{ab}^{IS} , is obtained by adding the correction term $\Delta C_{ab}(f_a, f_b)$ to C_{ab}^S , i.e.

$$C_{ab}^{IS}(f_a, f_b) = C_{ab}^S(f_a, f_b) + \Delta C_{ab}(f_a, f_b), \quad (7)$$

where ΔC_{ab} is defined as

$$\Delta C_{ab} = \Delta C_{ab}^T + \Delta C_{ab}^F, \quad (8)$$

with the test and field components of the correction term being

$$\Delta C_{ab}^T = \sum_{\ell=0}^L \sum_{k=0}^K \frac{m_a}{T_a} \frac{f_{Ma}}{\bar{\tau}_{ab}} c_\ell \Delta M_{ab}^{\ell k} L_\ell^{3/2}(s_a^2) \mathbf{v} \cdot \mathbf{u}_{ak}(f_a), \quad (9)$$

and

$$\Delta C_{ab}^F = \sum_{\ell=0}^L \sum_{k=0}^K \frac{m_a}{T_a} \frac{f_{Ma}}{\bar{\tau}_{ab}} c_\ell \Delta N_{ab}^{\ell k} L_\ell^{3/2}(s_a^2) \mathbf{v} \cdot \mathbf{u}_{bk}(f_b), \quad (10)$$

respectively. Here, $\bar{\tau}_{ab} = 3\sqrt{\pi}/(4v_{ab})$ is the collisional time between the colliding species a and b , with v_{ab} the associated collision frequency $v_{ab} = 4\sqrt{\pi}N_b q_a^2 q_b^2 \ln \Lambda / [3m_a^{1/2} T_a^{3/2}]$ (see Ref. 5). While the IS is derived in the limit $L \rightarrow \infty$ and $K \rightarrow \infty$, here we consider (L, K) to be two positive integers that we choose equal, i.e. $L = K$. Since previous neoclassical transport studies suggest that accurate friction coefficients in the Pfirsch-Schlüter regime require that $L = K \gtrsim 2$ (see Ref. 19), we consider the cases of $L = K = 2, 5$ and 10 . We note that the first neoclassical studies reported in Ref. 20 are performed with the like-species IS using $L = K = 1, 2$.

The quantities $\mathbf{u}_{ak}(f_a)$ appearing in Eqs. (9) and (10) are defined as the flow vectors and are expressed by¹⁹

$$\mathbf{u}_{ak}(f_a) = \frac{c_k}{n_a} \int d\mathbf{v} f_a L_k^{3/2}(s_a^2) \mathbf{v}, \quad (11)$$

with $c_k = 3 \cdot 2^k k! / (2k+3)!!$. Finally, we introduce the correction Braginskii matrix elements, $\Delta M_{ab}^{\ell k}$ and $\Delta N_{ab}^{\ell k}$, defined by

$$\Delta M_{ab}^{\ell k} = M_{ab}^{L\ell k} - M_{ab}^{S\ell k}, \quad (12a)$$

$$\Delta N_{ab}^{\ell k} = N_{ab}^{L\ell k} - N_{ab}^{S\ell k}, \quad (12b)$$

where the Braginskii matrices, $M_{ab}^{A\ell k}$ and $N_{ab}^{A\ell k}$ (being $A = L$ for Coulomb and $A = S$ for OS) are obtained from the test and field components of the operator collision model C_{ab}^{AT} and C_{ab}^{AF} , respectively, and are defined by^{19,25}

$$\frac{n_a}{\bar{\tau}_{ab}} M_{ab}^{A\ell k} = \int d\mathbf{v} v_{\parallel} L_{\ell}^{3/2}(s_a^2) C_{ab}^{AT} \left(f_{Ma} \frac{m_a v_{\parallel}}{T_a} L_k^{3/2}(s_a^2) \right), \quad (13a)$$

$$\frac{n_a}{\bar{\tau}_{ab}} N_{ab}^{A\ell k} = \int d\mathbf{v} v_{\parallel} L_{\ell}^{3/2}(s_a^2) C_{ab}^{AF} \left(f_{Mb} \frac{m_b v_{\parallel}}{T_b} L_k^{3/2}(s_b^2) \right), \quad (13b)$$

with $v_{\parallel} = \mathbf{b} \cdot \mathbf{v}$ the parallel component of the velocity along the magnetic field and $\mathbf{b} = \mathbf{B}/B$.

The Braginskii matrices $M_{ab}^{A\ell k}$ and $N_{ab}^{A\ell k}$ satisfy a set of relations stemming from the conservation laws and symmetries of the collision operator. In particular, from the momentum conservation law in Eq. (2b), one obtains that

$$M_{ab}^{A0k} + \frac{T_a v_{Ta}}{T_b v_{Tb}} N_{ba}^{A0k} = 0 \quad (k = 0, 1, 2, \dots). \quad (14)$$

In addition, in the case of collisions between particle species with the same temperatures ($T_a = T_b$), the Braginskii matrices admit symmetry properties because of the self-adjoint relations of C_{ab}^{TA} and C_{ab}^{FA} given in Eq. (4). From Eqs. (13) and (4), one obtains that

$$M_{ab}^{A\ell k} = M_{ab}^{Ak\ell}, \quad (15)$$

$$\frac{N_{ab}^{A\ell k}}{T_a v_{Ta}} = \frac{N_{ba}^{Ak\ell}}{T_b v_{Tb}} \quad (\ell, k = 0, 1, 2, \dots), \quad (16)$$

which implies that

$$\Delta M_{ab}^{A\ell k} = 0, \quad (17)$$

$$\Delta N_{ab}^{A\ell k} = \frac{N_{ab}^{A00} N_{ab}^{A\ell k} - N_{ab}^{A\ell 0} N_{ab}^{A0k}}{N_{Aak}^{00}} \quad (\ell, k = 0, 1, 2, \dots), \quad (18)$$

$$\Delta N_{ab}^{A00} = \Delta N_{ab}^{\ell 0} = \Delta N_{ab}^{A0k} = 0, \quad (19)$$

for $\ell, k = 1, 2, \dots$ in the case $T_a = T_b$. While the analytical expressions of the Braginskii matrices $M_a^{A\ell k}$ and $N_a^{A\ell k}$ up to $(\ell, k) \leq 2$ can be found in Ref. 17, we provide a new derivation of these coefficients here that allows us to extend them to arbitrary order (ℓ, k) in Sec. IV. This allows us to evaluate gyro-moment expansion of the IS for any (L, K) . Using these analytical expressions, we demonstrate numerically in Sec. VI that the relations and symmetry properties of the Braginskii matrices are satisfied.

III. SPHERICAL HARMONIC EXPANSION AND GYRO-AVERAGE OF THE IMPROVED SUGAMA OPERATOR

We expand the IS collision operator in terms of spherical harmonic particle moments in Sec. III A^{5,22}. This allow us to evaluate its gyro-average and to derive the GK and DK limits

Implementation of the Improved Sugama Collision Operator

of the IS collision operators in Secs. III B and III C, respectively. We notice that, while the GK form of the IS collision operator is presented in Ref. 17, here we follow a different methodology, which is based in the spherical harmonic technique used to obtain the GK and DK Coulomb collision operators in Ref. 5. This technique sheds some light on the analytical differences between the IS, OS and the Coulomb collision operators in the GK limit. Also, we note that the spherical harmonic expansion is particularly useful in deriving the expressions of the Braginskii matrix elements in Sec. IV.

A. Spherical Harmonic Expansion of the Improved Sugama Collision Operator

The perturbed particle distribution function, $f_a(\mathbf{r}, \mathbf{v})$, is expanded in the spherical harmonic basis according to^{5,22}

$$f_a(\mathbf{r}, \mathbf{v}) = f_{Ma} \sum_{p,j} \frac{1}{\sigma_j^p} \mathbf{M}_a^{pj}(\mathbf{r}) \cdot \mathbf{Y}^{pj}(\mathbf{s}_a), \quad (20)$$

with $\mathbf{s}_a = \mathbf{s}/v_{Ta}$ and $\sigma_j^p = p!(p+j+1/2)!/[2^p(p+1/2)!j!]$. In Eq. (20), the spherical harmonic basis is defined by $\mathbf{Y}^{pj}(\mathbf{s}_a) = \mathbf{Y}^p(\mathbf{s}_a)L_j^{p+1/2}(s_a^2)$, where we introduce the spherical harmonic tensors of order p , \mathbf{Y}^p , and the associated Laguerre polynomials, $L_j^{p+1/2}(s_a^2)$, defined in Eq. (6). The tensor \mathbf{Y}^p can be explicitly defined by introducing the spherical harmonic basis, \mathbf{e}^{pm} , that satisfies the orthogonality relation $\mathbf{e}^{pm} \cdot \mathbf{e}^{pm'} = (-1)^m \delta_{-m}^{m'}$ ²⁶, such that

$$\mathbf{Y}^p(\mathbf{s}_a) = s_a^p \sqrt{\frac{2\pi^{3/2} p!}{2^p(p+1/2)!}} \sum_{m=-p}^p Y_p^m(\xi, \theta) \mathbf{e}^{pm}, \quad (21)$$

where $Y_p^m(\xi, \theta)$ are the scalar harmonic functions. The spherical harmonic basis in Eq. (20), satisfies the orthogonality relation²⁶

$$\frac{1}{\pi^{3/2} \sigma_p^j} \int d\mathbf{s} e^{-s^2} L_j^{p+1/2}(s^2) \mathbf{Y}^{p'}(\mathbf{s}) L_{j'}^{p'+1/2}(s^2) \mathbf{Y}^p(\mathbf{s}) \cdot \mathbf{T}^p = \delta_{pp'} \delta_{jj'} \mathbf{T}^p, \quad (22)$$

with \mathbf{T}^p an arbitrary p -th order tensor. From the orthogonality relation in Eq. (22), it follows that the spherical harmonic particle moments $\mathbf{M}_a^{pj}(\mathbf{r})$ are defined as

$$\mathbf{M}_a^{pj}(\mathbf{r}) = \frac{1}{n_a} \int d\mathbf{v} f_a(\mathbf{r}, \mathbf{v}) \mathbf{Y}^{pj}(\mathbf{s}_a). \quad (23)$$

Here, we emphasize that the spherical harmonic particle moments depend on the particle position \mathbf{r} only.

We now use the definition of the spherical harmonic particle moments, \mathbf{M}_a^{pj} given Eq. (37), and relate them to the flow vectors expressed in Eq. (11), to obtain the spherical harmonic expansion of the IS collision operator. Therefore, from Eq. (11) and noticing that $\mathbf{s}_a = \mathbf{Y}^1(\mathbf{s}_a)$, we derive

$$\begin{aligned} \mathbf{u}_{ak}(f_a) &= \frac{c_k v_{Ta}}{n_a} \int d\mathbf{v} f_a L_k^{3/2}(s_a^2) \mathbf{Y}^1(\mathbf{s}_a) \\ &= c_k v_{Ta} \mathbf{M}_a^{1k}(\mathbf{r}). \end{aligned} \quad (24)$$

Inserting Eq. (24) into Eqs. (9) and (10) yields the spherical harmonic expansion of the IS collision operator, which is useful to evaluate its GK limit.

B. Gyrokinetic Improved Sugama Collision Operator

We now consider the GK limit of the IS collision operator where the fast particle gyro-motion is analytically averaged out. Contrary to the IS collision operator, defined on the particle phase-space $\mathbf{z} = (\mathbf{r}, \mathbf{v})$ (see Eq. (7)), the GK IS collision operator, which we denote by \mathcal{C}_{ab}^{IS} , is defined on the gyrocenter phase-space coordinates $\mathbf{Z} = (\mathbf{R}, \mu, v_{\parallel}, \theta, t)$ where \mathbf{R} is the gyrocenter position, $\mu = mv_{\perp}^2/[2B]$ is the magnetic moment and θ is the gyroangle. More precisely, \mathcal{C}_{ab}^{IS} , is obtained by performing the gyro-average of the IS collision operator C_{ab}^{IS} , i.e.

$$\mathcal{C}_{ab}^{IS} = \left\langle C_{ab}^{IS} \right\rangle_{\mathbf{R}} = \int_0^{2\pi} \left| \frac{d\theta}{2\pi} C_{ab}^{IS}(\mathbf{z}(\mathbf{Z})) \right|. \quad (25)$$

where the integral over the gyroangle appearing in Eq. (25) is performed holding \mathbf{R} constant (while collisions occur at the particle position \mathbf{r}). In general, the coordinate transformation that relates the gyrocenter and particles coordinates, \mathbf{Z} and \mathbf{z} respectively, can be written as $\mathbf{Z} = \mathbf{z} + \delta\mathbf{z}$,

Implementation of the Improved Sugama Collision Operator

where δz are functions of phase-space coordinates and perturbed fields and contain terms at all orders in the GK expansion parameter $\epsilon \sim e\phi/T_e$ (ϕ being the small amplitude and small scale electrostatic fluctuating potential^{5,27}). At the lowest order in the GK expansion, the coordinate transformation reduces to $\delta v_{\parallel} = \delta\mu = \delta\theta = 0$ and $\delta r \simeq -\rho_a$. Hence, the IS collision operator can be gyro-averaged holding \mathbf{R} constant by using the transformation $\mathbf{r} = \mathbf{R}(\mathbf{r}, \mathbf{v}) + \boldsymbol{\rho}_a(\mathbf{r}, \mathbf{v})^{21}$.

Focusing first on the test component of ΔC_{ab}^T , we perform the gyro-average in Eq. (25) using $\mathbf{r} = \mathbf{R}(\mathbf{r}, \mathbf{v}) + \boldsymbol{\rho}_a(\mathbf{r}, \mathbf{v})$ in the spatial argument of $\mathbf{M}_a^{1k}(\mathbf{r})$, such that in Fourier space it yields $\mathbf{M}_a^{1k}(\mathbf{r}) = \int d\mathbf{k} \mathbf{M}_a^{1k}(\mathbf{k}) e^{i\mathbf{k}\cdot\mathbf{R}} e^{i\mathbf{k}\cdot\boldsymbol{\rho}_a}$. For a single Fourier component, we derive

$$\begin{aligned} \Delta \mathcal{C}_{ab}^T &= \sum_{\ell=0}^L \sum_{k=0}^K \frac{m_a}{T_a} \frac{f_{Ma}}{\bar{\tau}_{ab}} c_{\ell} c_k v_{Ta} \Delta M_{ab}^{\ell k} L_{\ell}^{3/2} (s_a^2) e^{i\mathbf{k}\cdot\mathbf{R}} \\ &\quad \times \left\langle e^{i\mathbf{k}\cdot\boldsymbol{\rho}_a} \mathbf{v} \cdot \mathbf{M}_a^{1k}(\mathbf{k}) \right\rangle_{\mathbf{R}} \\ &= \sum_{\ell=0}^L \sum_{k=0}^K \frac{m_a}{T_a} \frac{f_{Ma}}{\bar{\tau}_{ab}} c_{\ell} c_k v_{Ta} \Delta M_{ab}^{\ell k} L_{\ell}^{3/2} (s_a^2) e^{i\mathbf{k}\cdot\mathbf{R}} \\ &\quad \times \left[v_{\parallel} J_{0a} \mathbf{b} \cdot \mathbf{M}_a^{1k}(\mathbf{k}) + i v_{\perp} J_{1a} \mathbf{e}_2 \cdot \mathbf{M}_a^{1k}(\mathbf{k}) \right], \end{aligned} \quad (26)$$

where we introduce the basis vectors $(\mathbf{e}_1, \mathbf{e}_2)$, such that $\mathbf{v}_{\perp} = v_{\perp} (\mathbf{e}_2 \cos \theta - \mathbf{e}_1 \sin \theta)$. Additionally, $J_{0a} = J_0(b_a \sqrt{x_a})$ and $J_{1a} = J_1(b_a \sqrt{x_a})$ are the zeroth and first order Bessel functions (with $b_a = k_{\perp} \rho_a$ the normalized perpendicular wavenumber and $x_a = v_{\perp}^2 / v_{Ta}^2$), resulting from the presence of FLR effects in the IS collision operator.

We now relate the spherical harmonic moments \mathbf{M}_a^{1k} of the perturbed particle to the gyrocenter perturbed distribution functions. More precisely, we express the \mathbf{M}_a^{1k} in terms of the nonadiabatic part, h_a , of the perturbed gyrocenter distribution function g_a . The two gyrocenter distribution functions, h_a and g_a , are related by⁵

$$h_a(\mathbf{R}, \mu, v_{\parallel}) = g_a(\mathbf{R}, \mu, v_{\parallel}) + \frac{q_a}{T_a} F_{Ma} \langle \phi \rangle_{\mathbf{R}}, \quad (27)$$

in the electrostatic limit. Here, F_{Ma} is the gyrocenter Maxwellian distribution function. The perturbed particle distribution function f_a is related to the perturbed gyrocenter distribution function g_a by the scalar invariance of the full particle and gyrocenter distribution functions, i.e.

$$f_a(\mathbf{r}, \mathbf{v}) = g_a(\mathbf{R}, \mu, v_{\parallel}) + F_{Ma}(\mathbf{R}, \mu, v_{\parallel}) - f_{Ma}(\mathbf{r}(\mathbf{Z}), \mathbf{v}(\mathbf{Z})). \quad (28)$$

Using the pull-back operator \mathcal{T} , such that the functional forms of f_{Ma} and F_{Ma} are related by $f_{Ma} = \mathcal{T}F_{Ma}$ ²¹, we derive that

$$f_a(\mathbf{r}, \mathbf{v}) = g_a(\mathbf{R}, \mu, v_{\parallel}) + (F_{Ma} - \mathcal{T}F_{Ma})(\mathbf{Z}) = g_a^{gc}(\mathbf{Z}). \quad (29)$$

We remark that, while both g_a and h_a are gyrophase independent functions, g_a^{gc} is gyrophase dependent. An expression of the pull-back transformation \mathcal{T} can be obtained at the leading order in the GK expansion parameter $\varepsilon \sim e\phi/T_e$, yielding⁵

$$\begin{aligned} f_a(\mathbf{r}, \mathbf{v}) &= g_a^{gc}(\mathbf{Z}(z)) \\ &= g_a(\mathbf{R}(\mathbf{r}, \mathbf{v}), \mu, v_{\parallel}) - \frac{q_a}{T_a} F_{Ma}(\phi(\mathbf{r}) - \langle \phi \rangle_{\mathbf{R}}) + O(\varepsilon^2) \\ &= h_a(\mathbf{R}(\mathbf{r}, \mathbf{v}), \mu, v_{\parallel}) - \frac{q_a}{T_a} \phi(\mathbf{r}) F_{Ma} + O(\varepsilon^2), \end{aligned} \quad (30)$$

being $\mathbf{r} = \mathbf{R} + \boldsymbol{\rho}_a(\mu, \theta)$. Using Eq. (30) allows us to finally express \mathbf{M}_a^{1k} in terms of h_a ,

$$\begin{aligned} v_{Ta} \mathbf{M}_a^{1k}(\mathbf{r}) &= \frac{v_{Ta}}{n_a} \int d\mathbf{v} f_a(\mathbf{r}, \mathbf{v}) L_k^{3/2}(s_a^2) \mathbf{Y}^1(s_a) \\ &= \frac{1}{n_a} \int d\mathbf{v} \int d\mathbf{r}' \delta(\mathbf{r}' - \mathbf{r}) f_a(\mathbf{r}', \mathbf{v}) L_k^{3/2}(s_a^2) \mathbf{v} \\ &= \frac{1}{N_a} \int d\mathbf{R} dv_{\parallel} d\mu d\theta \frac{B}{m_a} (\mathbf{R} + \boldsymbol{\rho}_a - \mathbf{r}) \\ &\quad \times h_a(\mathbf{R}(\mathbf{r}, \mathbf{v}), \mu, v_{\parallel}) L_k^{3/2}(s_a^2) \mathbf{v} \\ &= \frac{e^{ik \cdot r}}{N_a} \int dv_{\parallel} d\mu d\theta \frac{B}{m_a} L_k^{3/2}(s_a^2) \\ &\quad \times h_a(\mathbf{k}, \mu, v_{\parallel}) (b v_{\parallel} J_{0a} - i v_{\perp} e_2 J_{1a}). \end{aligned} \quad (31)$$

We remark that the contribution from the terms proportional to ϕ , appearing in Eq. (30), are

Implementation of the Improved Sugama Collision Operator

neglected in Eq. (31). In fact, while these terms are of the same order as h_a (i.e. they are order ε), they yield a small contribution in the collision operator¹². We neglect them here, but notice that their contributions to the Coulomb collision operator are included in Ref. 5 and have little effects at the gyroradius scale. With Eqs. (31) and (26), the GK test component of the correction term , $\Delta\mathcal{C}_{ab}^T = \langle \Delta C_{ab}^T \rangle_R$, can be obtained in terms of the gyrocenter distribution function h_a .

Focusing on the field component of $\Delta\mathcal{C}_{ab}$, i.e. $\Delta\mathcal{C}_{ab}^F$, we remark that a similar derivation of its expression can be carried out as for $\Delta\mathcal{C}_{ab}^T$. In particular, the expression of the spherical harmonic moment with \mathbf{M}_b^{1k} , appearing in Eq. (10), is obtained with Eq. (31) having replaced a with b .

Hence, the GK IS collision operator can be expressed as¹⁷

$$\mathcal{C}_{ab}^{IS} = \mathcal{C}_{ab}^S + \Delta\mathcal{C}_{ab}^T + \Delta\mathcal{C}_{ab}^F, \quad (32)$$

where \mathcal{C}_{ab}^S is the OS GK collision operator, given in Ref. 12, and $\Delta\mathcal{C}_{ab}^T$ and $\Delta\mathcal{C}_{ab}^F$ given by

$$\begin{aligned} \Delta\mathcal{C}_{ab}^T &= \sum_{\ell=0}^L \sum_{k=0}^K \frac{c_\ell}{\bar{\tau}_{ab}} \frac{m_a F_{Ma}}{T_a} L_\ell^{3/2}(s_a^2) \Delta M_{ab}^{\ell k} \\ &\times \left(\bar{u}_{\parallel a}^k(h_a) J_{0a} v_\parallel + \bar{u}_{\perp a}^k(h_a) J_{1a} v_\perp \right), \end{aligned} \quad (33a)$$

$$\begin{aligned} \Delta\mathcal{C}_{ab}^F &= \sum_{\ell=0}^L \sum_{k=0}^K \frac{c_\ell}{\bar{\tau}_{ab}} \frac{m_a F_{Ma}}{T_a} L_\ell^{3/2}(s_a^2) \Delta N_{ab}^{\ell k} \\ &\times \left(\bar{u}_{\parallel b}^k(h_b) J_{0a} v_\parallel + \bar{u}_{\perp b}^k(h_b) J_{1a} v_\perp \right). \end{aligned} \quad (33b)$$

where we introduce the quantities

$$\bar{u}_{\parallel s}^k(h_s) = \frac{c_k}{n_s} \int dv_\parallel d\mu d\theta \frac{B}{m_s} L_k^{3/2}(s_s^2) h_s J_{0s} v_\parallel, \quad (34a)$$

$$\bar{u}_{\perp s}^k(h_s) = \frac{c_k}{n_s} \int dv_\parallel d\mu d\theta \frac{B}{m_s} L_k^{3/2}(s_s^2) h_s J_{1s} v_\perp. \quad (34b)$$

As an aside, we remark that, while the correction term in the IS collision operator contains only velocity space integrals in both the test and field components (see Eq. (11)), velocity derivatives evaluated at the particle position \mathbf{r} are contained in the test part of the OS collision operator, yielding pitch-angle scattering and energy diffusion in velocity space. The GK limit of these

velocity derivatives is often obtained by using the lowest-order gyrocenter coordinates and having replaced f_a by the nonadiabatic part of the distribution function h_a ¹². More precisely, using the chain rule and holding \mathbf{r} constant, one derives

$$\begin{aligned} \frac{\partial}{\partial \mathbf{v}} \Big|_{\mathbf{r}} f_a &\simeq \mathbf{b} \frac{\partial}{\partial v_{\parallel}} h_a + \frac{m_a \mathbf{v}_{\perp}}{B} \frac{\partial}{\partial \mu} h_a \\ &\quad - \frac{\partial \rho_a}{\partial \mathbf{v}} \Big|_{\mathbf{r}} \cdot \frac{\partial}{\partial \mathbf{R}} h_a, \end{aligned} \quad (35)$$

where the gyrophase independence of h_a is used. We estimate the last term in Eq. (35) to be order of $k_{\perp} \rho_a$ in Fourier space. In particular, a FLR term of the order of $\sim v_{ab} k_{\perp}^2 \rho_a^2 h_a$ appear in the test component of the GK OS collision operator¹² (and, hence, in the GK IS operator), such that it becomes large at smaller scales and/or high collisionality. As a consequence, the field component of the GK OS collision operator becomes negligible compared to the test part when $k_{\perp} \rho_a \gg 1$, as a result of the approximation in Eq. (35).

The spherical harmonic approach used to derive the GK Coulomb collision operator in Ref. 5, allows for the evaluation and gyro-average of the velocity derivatives at the particle position without expanding the latter as in Eq. (35). In particular, the velocity derivatives are applied to f_a rather than h_a in the spherical harmonic approach (in contrast, therefore, to Ref. 12), such that they are not transformed into gyrocenter coordinates as in Eq. (35). Then, the particles velocity-space derivatives, expressed in terms of the spherical harmonic moment \mathbf{M}_a^{pj} , can be related to h_a inserting Eq. (30) into Eq. (37). This yields FLR terms proportional to Bessel functions J_{na} , which oscillates and decreases in amplitude when $k_{\perp} \rho_a$ becomes large, such that $J_{na} \sim \sqrt{2\Omega_a / [\pi k_{\perp} v_{\perp}]} \cos(k_{\perp} v_{\perp} / \Omega_a - n\pi/2 - \pi/4)$ for large argument $k_{\perp} v_{\perp} / \Omega_a$. The same dependence is found in the field component of the Coulomb collision operator. These differences in the analytical derivations of the GK Coulomb and GK OS collision operators yields inherent deviations also at small k_{\perp} in the high-collisionality case.

C. Drift-Kinetic Improved Sugama Collision Operator

We now derive the DK IS operator from the GK IS collision operator, given in Eq. (32), by neglecting the difference between the particle and gyrocenter position, such that $\mathbf{r} \simeq \mathbf{R}$. Hence,

Implementation of the Improved Sugama Collision Operator

the DK IS collision operator is derived in the zero gyroradius limit of the GK IS operator approximating $J_{0s} \simeq 1$, $J_{1s} = 0$ and $f_s \simeq g_s$ (see Eq. (27)). The DK OS is given in Ref. 5 and the DK limits of the GK test and field components of $\Delta\mathcal{C}_{ab}$ are

$$\Delta\mathcal{C}_{ab}^T = \sum_{\ell=0}^L \sum_{k=0}^K \frac{m_a}{T_a} \frac{F_{Ma}}{\bar{\tau}_{ab}} c_\ell c_k v_{Ta} L_\ell^{3/2}(s_a^2) \Delta M_{ab}^{\ell k} v_{\parallel} \mathbf{b} \cdot \mathbf{M}_a^{1k}, \quad (36a)$$

$$\Delta\mathcal{C}_{ab}^F = \sum_{\ell=0}^L \sum_{k=0}^K \frac{m_a}{T_a} \frac{F_{Ma}}{\bar{\tau}_{ab}} c_\ell c_k v_{Tb} L_\ell^{3/2}(s_a^2) \Delta N_{ab}^{\ell k} v_{\parallel} \mathbf{b} \cdot \mathbf{M}_b^{1k}, \quad (36b)$$

respectively. In Eq. (36), the spherical particle moments, \mathbf{M}_s^{1k} ($s = a, b$), are expressed in terms of g_s , such that

$$\mathbf{b} \cdot \mathbf{M}_s^{1k} = \frac{1}{N_s} \int d\mu dv_{\parallel} d\theta \frac{B}{m_s} g_s L_k^{3/2}(s_s^2) \frac{v_{\parallel}}{v_{Ts}}. \quad (37)$$

The GK and DK expressions of the IS collision operator, given in Eqs. (33) and (36), can be implemented in continuum GK codes using a discretization scheme in velocity-space (e.g., based on a finite volume approach²⁸ or a finite difference scheme²⁰) to evaluate numerically the velocity-integrals. In this work, we use a gyro-moment approach to carry out these velocity integrals and implement these operators numerically. For this purpose, we derive closed analytical expressions of the Braginskii matrices, required to evaluate the quantities $\Delta M_{ab}^{\ell k}$ and $\Delta N_{ab}^{\ell k}$, in the next section.

IV. BRAGINKSII MATRICES

In order to evaluate the correction term ΔC_{ab} given in Eq. (8), analytical expressions for the Braginskii matrices, M_{ab}^{Ajk} and N_{ab}^{Ajk} , associated with the Coulomb and OS collision operators are derived. This extends the evaluation of the $(\ell, k) \leq 2$ Braginskii matrices reported in Ref. 17 to arbitrary (ℓ, k) . For this calculation, we leverage the spherical harmonic expansions of the Coulomb and OS collision operators presented in Ref. 5. More precisely, we use the spherical harmonic expansion of f_a (see Sec. III A) to obtain the Braginskii matrices of the Coulomb and OS collision operators in Secs. IV A and IV B, respectively.

A. Braginskii Matrix of the Coulomb Collision Operator

We first derive the Braginskii matrix associated with the Coulomb collision operator, namely $M_{ab}^{L\ell k}$ and $N_{ab}^{L\ell k}$, appearing in Eq. (12). For this purpose, we use the expansion of the perturbed particle distribution function, given in Eq. (20), to obtain the spherical harmonic expansion of the test and field components of the Coulomb collision operator, C_{ab}^{LT} and C_{ab}^{LF} , derived in Ref. 5. These expressions, reported here, are given by

$$C_{ab}^{LT}(\mathbf{r}, \mathbf{v}) = \sum_{p=0}^{\infty} \sum_{j=0}^{\infty} \frac{f_{Ma}}{\sigma_j^p} \mathbf{M}_a^{pj}(\mathbf{r}) \cdot \mathbf{Y}^p(\hat{\mathbf{v}}) v_{ab}^{Tpj}(v), \quad (38a)$$

$$C_{ab}^{LF}(\mathbf{r}, \mathbf{v}) = \sum_{p=0}^{\infty} \sum_{j=0}^{\infty} \frac{f_{Ma}}{\sigma_j^p} \mathbf{M}_b^{pj}(\mathbf{r}) \cdot \mathbf{Y}^p(\hat{\mathbf{v}}) v_{ab}^{Fpj}(v), \quad (38b)$$

where the expressions of the test and field speed functions, $v_{ab}^{Tpj}(v)$ and $v_{ab}^{Fpj}(v)$, can be found in the Appendix A of Ref. 5. We first use the expression of C_{ab}^{LT} in Eq. (38b) to evaluate M_{ab}^{Ljk} (see Eq. (13a)). We remark that the GK Coulomb collision operator, which we compare with the GK IS operator in Sec. VI, is derived in Ref. 5 by gyro-averaging Eq. (38) according to Eq. (25).

By inserting $f_a = f_{Ma} m_a v_{\parallel} L_k^{3/2}(s_a^2)/T_a$ (see Eq. (20)) into the C_{ab}^{LT} and by noticing that $\mathbf{Y}^1(s_a) = \mathbf{v}/v_{Ta}$, we obtain the $p = 1$ term of Eq. (38), i.e.

$$C_{ab}^{LT} \left(f_{Ma} \frac{m_a v_{\parallel}}{T_a} L_k^{3/2}(s_a^2) \right) = \frac{2 f_{Ma}}{v_{Ta}} \frac{v_{\parallel}}{v} v_{ab}^{T1k}(v). \quad (39)$$

Then, the matrix element $M_{ab}^{L\ell k}$, defined in Eq. (13a), can be computed by expanding the associated Laguerre polynomial using Eq. (6) with $p = 1$ and by performing the velocity integrals over the speed function $v_{ab}^{T1k}(v)$. It yields

$$M_{ab}^{L\ell k} = \sum_{l=0}^{\ell} \frac{2}{3} \frac{\bar{\tau}_{ab}}{n_a} L_{\ell l}^1 \bar{v}_{*ab}^{T1kl}. \quad (40)$$

A similar derivation can be carried out to evaluate N_{ab}^{Ljk} (see Eq. (13b)) by using the expression of C_{ab}^{LF} in Eq. (38b), i.e.

$$N_{ab}^{L\ell k} = \sum_{l=0}^{\ell} \frac{2}{3} \frac{\bar{\tau}_{ab}}{n_a} \chi_{ab} L_{\ell l}^1 \bar{v}_{*ab}^{F1kl}, \quad (41)$$

with $\chi_{ab} = v_{Ta}/v_{Tb}$ the ratio between the thermal velocities. The closed analytical expressions of test and field speed integrated functions \bar{v}_{*ab}^{T1kl} and \bar{v}_{*ab}^{F1kl} appearing in Eqs. (40) and (41), respectively, are given in Ref. 5. Eqs. (40) and (41) allows for the evaluation of the terms associated with the Coulomb collision operator appearing in the correction matrix elements, ΔM_{ab}^{jk} and ΔN_{ab}^{jk} defined in Eq. (12). They are evaluated in terms of mass and temperature ratios of the colliding species.

B. Braginskii Matrix of the Original Sugama Collision Operator

We now evaluate the Braginskii matrix associated with the OS collision operator, namely $M_{ab}^{S\ell k}$ and $N_{ab}^{S\ell k}$, appearing in Eq. (12). For $f_a = f_{Ma} m_a v_{\parallel} L_k^{3/2}(s_a^2)/T_a$, using the spherical harmonic expansion of the OS operator in Ref. 5, the test component of the OS collision operator yields

$$C_{ab}^{TS} \left(f_{Ma} L_k^{3/2}(s_a^2) \frac{m_a v_{\parallel}}{T_a} \right) = \frac{2}{v_{Ta}} f_{Ma} \frac{v_{\parallel}}{v} v_{ab}^{S1k}(v) + \sum_{i=1}^3 X_{ab}^i, \quad (42)$$

where the quantities X_{ab}^i are defined by

$$X_{ab}^1 = -\frac{16}{3\sqrt{\pi}} (1 + \chi_{ab}^2) (\theta_{ab} - 1) f_{Ma} \frac{m_a v_{\parallel}}{T_a} \sum_{l=0}^k L_{kl}^1 \bar{v}_{ab}^{\parallel l+3}, \quad (43a)$$

$$X_{ab}^2 = -2(1 + \chi_{ab}^2) (\theta_{ab} - 1) \frac{m_a}{T_a} u_{\parallel a}^k v_{\parallel} f_{Ma} v_{ab}^{\parallel}(v) s_a^2, \quad (43b)$$

$$X_{ab}^3 = -\frac{2}{\tau_{ab}} f_{Ma} \frac{\chi_{ab} (\theta_{ab} - 1)^2}{\sqrt{1 + \chi_{ab}^2}} \frac{m_a}{T_a} v_{\parallel} u_{\parallel a}^k, \quad (43c)$$

with $v_{ab}^{S1k}(v)$ the velocity dependent speed function (whose expression is given in Ref. 5), being $\bar{v}_{ab}^{\parallel k} = \int_0^\infty ds_a s_a^{2k} v_{ab}^{\parallel}(v) e^{-s_a^2}$ (with $v_{ab}^{\parallel}(v) = 2v_{ab} [\text{erf}(s_b) - s_b \text{erf}'(s_b)] / (2s_b^2 s_a^3)$ the velocity dependent energy diffusion frequency, and $u_{\parallel a}^k = 4/(3\sqrt{\pi})(k+3/2)!/k! \delta_k^0$). In deriving Eq. (42), we remark that the terms proportional to the perturbed temperature, $\delta T_a(f_a) = T_a \int d\mathbf{v} f_a (2s_a^2/3 - 1) / n_a$, vanish exactly when applied to $f_a = f_{Ma} m_a v_{\parallel} L_k^{3/2}(s_a^2)/T_a$ because of the velocity integration over the pitch-angle variable v_{\parallel}/v .

Similarly, the field component of the OS collision for $f_b = f_{Mb} m_b v_{\parallel} L_k^{3/2}(s_b^2)/T_b$ yields

$$C_{ab}^{FS} \left(f_{Mb} L_k^{3/2}(s_b^2) \frac{m_b v_{\parallel}}{T_a} \right) = \frac{2\theta_{ab}}{\bar{\tau}_{ab}} (1 + \chi_{ab}^2) f_{Ma} \frac{m_a v_{\parallel}}{T_a} \\ \times \left[\frac{3\sqrt{\pi}}{2} \frac{\Phi(s_b)}{s_a} + \frac{\chi_{ab}(\theta_{ab} - 1)}{(1 + \chi_{ab}^2)^{3/2}} \right] V_{ab} \left(f_{Mb} L_k^{3/2}(s_b^2) \frac{m_b v_{\parallel}}{T_b} \right), \quad (44)$$

where

$$V_{ab} \left(f_{Mb} L_k^{3/2}(s_b^2) \frac{m_b v_{\parallel}}{T_b} \right) = -\frac{\theta_{ba}}{\bar{\tau}_{ba}} (1 + \chi_{ba}^2) \frac{m_b}{\gamma_{ab}} \\ \times \int d\mathbf{v} L_k^{3/2}(s_b^2) \frac{m_b v_{\parallel}^2}{T_b} f_{Mb} \left[\frac{3\sqrt{\pi}}{2} \frac{\Phi(s_a)}{s_b} + \frac{\chi_{ba}(\theta_{ba} - 1)}{(1 + \chi_{ba}^2)^{3/2}} \right], \quad (45)$$

with $\Phi(x) = [\text{erf}(x) - x \text{erf}'(x)] / (2x^2)$. The velocity integral in Eq. (45) can be performed analytically using Eq. (6), and leads to

$$V_{ab} \left(f_{Mb} L_k^{3/2}(s_b^2) \frac{m_b v_{\parallel}}{T_b} \right) = \frac{m_b}{\gamma_{ab}} \mathcal{V}_{ab}^l, \quad (46)$$

with the following definition

$$\mathcal{V}_{ab}^l = -2\theta_{ab}(1 + \chi_{ab}^2) \frac{n_b}{\bar{\tau}_{ab}} \left[\frac{1}{2} \frac{\chi_{ab}(\theta_{ab} - 1)}{(1 + \chi_{ab}^2)^{3/2}} u_{\parallel a}^l \right. \\ \left. + \sum_{m=0}^l L_{lm}^1 \left(\frac{1}{\chi_{ab}^2} E_{ab}^m - \frac{1}{\chi_{ab}} e_{ab}^{m+1} \right) \right], \quad (47)$$

where we introduce $e_{ba}^k = \int_0^\infty ds_b s_b^{2k} \text{erf}'(s_a) e^{-s_b^2}$ and $E_{ba}^k = \int_0^\infty ds_b s_b^{2k+1} \text{erf}(s_a) e^{-s_b^2}$. The test and field components of the OS collision operator, given in Eqs. (42) and (44), are now in a suitable form to evaluate the analytical expressions of $M_{ab}^{S\ell k}$ and $N_{ab}^{S\ell k}$ defined by Eq. (13).

Starting with the Braginskii matrix element associated with C_{ab}^{TS} , the velocity integral in M_{ab}^{Sjk} , given in Eq. (13a), is evaluated using the series expansion of the associated Laguerre polynomials, Eq. (6). Thus, we derive

$$M_{ab}^{S\ell k} = \sum_{n=1}^3 M_{abn}^{S\ell k}, \quad (48)$$

where we introduce the quantities

$$M_{ab1}^{S\ell k} = \frac{\bar{\tau}_{ab}}{n_a} \sum_{l=0}^{\ell} \frac{2}{3} L_{\ell l}^1 \bar{v}_{*ab}^{S1kl}, \quad (49a)$$

$$\begin{aligned} M_{ab2}^{S\ell k} = & -\frac{16}{3\sqrt{\pi}} \bar{\tau}_{ab} (\theta_{ab} - 1) (1 + \chi_{ab}^2) \\ & \times \left[u_{\parallel a}^k \sum_{l=0}^{\ell} L_{\ell l}^1 \bar{v}_{ab}^{\parallel l+3} + u_{\parallel a}^{\ell} \sum_{l=0}^k L_{kl}^1 \bar{v}_{ab}^{\parallel l+3} \right], \end{aligned} \quad (49b)$$

$$M_{ab3}^{S\ell k} = -\frac{2\chi_{ab}(\theta_{ab} - 1)^2}{\sqrt{1 + \chi_{ab}^2}} u_{\parallel a}^k u_{\parallel a}^{\ell}. \quad (49c)$$

In Eq. (49a), the analytical expression of the speed integrated function, \bar{v}_{*ab}^{S1kl} , is reported in Ref. 5. Similarly for $N_{ab}^{S\ell j}$, using Eq. (44) and employing the expansion of the associated Laguerre polynomials in Eq. (6) yield

$$N_{ab}^{S\ell k} = -\frac{2\bar{\tau}_{ab}}{n_a} \frac{m_b}{\gamma_{ab}} \mathcal{V}_{ba}^k \mathcal{V}_{ab}^{\ell}. \quad (50)$$

The Braginskii matrix elements associated with the Coulomb collision operator, given in Eqs. (40) and (41), and the ones associated with the OS operator, given in Eqs. (48) and (50), allow us to obtain the correction Braginskii matrix elements $\Delta M_{ab}^{\ell k}$ and $\Delta N_{ab}^{\ell k}$ for arbitrary (ℓ, k) .

V. GYRO-MOMENT EXPANSION OF THE IMPROVED SUGAMA COLLISION OPERATOR

We now project the GK and DK IS collision operators onto a Hermite-Laguerre polynomial basis, a technique that we refer to as the gyro-moment approach. Previous works^{5,16,29} demonstrate the advantage of the gyro-moment approach in modelling the plasma dynamics in the boundary region, where the time evolution of the gyro-moments is obtained by projecting the GK Boltzmann equation onto the Hermite-Laguerre basis yielding an infinite set of fluid-like equations²¹. At

Implementation of the Improved Sugama Collision Operator

high-collisionality, high-order gyro-moments are damped such that only the lowest-order ones are sufficient to evolve the dynamics. As a consequence, in these conditions, the gyro-moment hierarchy can be reduced to a fluid model where collisional effects are obtained using the Hermite-Laguerre expansion of advanced collision operators at the lowest order in the ratio between the particle mean-free-path to the parallel scale length. As an example of these fluid models, we evaluate the lowest-order terms of the gyro-moment expansions of the DK IS, OS and Coulomb collision operators that enter in the evolution equations of the fluid quantities in Sec. A.

Since the gyro-moment expansion of the OS GK and DK Sugama collision operator is obtained in Ref. 5 (and was benckmarked with the GK GENE code), we focus here on the projections of the corrections $\Delta\mathcal{C}_{ab}^T$ and $\Delta\mathcal{C}_{ab}^F$, given in Eq. (33). The GK IS collision operator \mathcal{C}_{ab}^{IS} is formulated for h_a , the non-adiabatic part of the perturbed gyrocenter distribution function g_a (see Eq. (27)). Therefore, we expand the collision operator in terms of gyro-moments of h_a . More precisely, h_a is written as

$$h_a = \sum_{p=0}^{\infty} \sum_{j=0}^{\infty} n_a^{pj} \frac{H_p(s_{\parallel a}) L_j(x_a)}{\sqrt{2^p p!}} F_{Ma}, \quad (51)$$

with $s_{\parallel a} = v_{\parallel}/v_{Ta}$. In Eq. (51), the Hermite and Laguerre polynomials, H_p and L_j , are defined via their Rodrigues' formulas $H_p(x) = (-1)^p e^{x^2} d^p (e^{-x^2}) / dx^p$ and $L_j(x) = e^x / j! d^j (e^{-x} x^j) / dx^j$, and are orthogonal over the intervals, $]-\infty, \infty[$ weighted by e^{-x^2} , and $[0, +\infty[$ weighted by e^{-x} , respectively, such that

$$\int_{-\infty}^{\infty} dx H_p(x) H_{p'}(x) e^{-x^2} = 2^p p! \sqrt{\pi} \delta_p^{p'}, \quad (52)$$

$$\int_0^{\infty} dx L_j(x) L_{j'}(x) e^{-x} = \delta_j^{j'}. \quad (53)$$

Because of the orthogonality relations in Eq. (52), the non-adiabatic gyro-moments of h_a , n_a^{pj} , are defined by

$$n_a^{pj} = \frac{1}{N_a} \int d\mu dv_{\parallel} d\theta \frac{B}{m_a} h_a \frac{H_p(s_{\parallel a}) L_j(x_a)}{\sqrt{2^p p!}}. \quad (54)$$

where N_a is the gyrocenter density and F_{Ma} the gyrocenter Maxwellian distribution function. We detail the projection of the GK IS collision operator in Sec. V A, and obtain the DK limit of the same operator in Sec. V B in terms of n_a^{pj} .

A. Expansion of the GK IS Collision Operator

We first derive the gyro-moment expansion of the GK IS collision operator in Eq. (32), that is

$$\mathcal{C}_{ab}^{ISpj} = \mathcal{C}_{ab}^{Spj} + \Delta\mathcal{C}_{ab}^{Tpj} + \Delta\mathcal{C}_{ab}^{Fpj}. \quad (55)$$

where the Hermite-Laguerre projection of \mathcal{C}_{ab}^{IS} is defined by

$$\mathcal{C}_{ab}^{ISpj} = \frac{1}{N_a} \int d\mu dv_{\parallel} d\theta \frac{B}{m_a} \mathcal{C}_{ab}^{IS} \frac{H_p(s_{\parallel a}) L_j(x_a)}{\sqrt{2^p p!}}, \quad (56)$$

and similar definitions are used for the remaining terms in Eq. (55), in particular

$$\Delta\mathcal{C}_{ab}^{Tpj} = \frac{1}{N_a} \int d\mu dv_{\parallel} d\theta \frac{B}{m_a} \Delta\mathcal{C}_{ab}^T \frac{H_p(s_{\parallel a}) L_j(x_a)}{\sqrt{2^p p!}} \quad (57)$$

and

$$\Delta\mathcal{C}_{ab}^{Fpj} = \frac{1}{N_a} \int d\mu dv_{\parallel} d\theta \frac{B}{m_a} \Delta\mathcal{C}_{ab}^F \frac{H_p(s_{\parallel a}) L_j(x_a)}{\sqrt{2^p p!}}. \quad (58)$$

Since the expression of \mathcal{C}_{ab}^{Spj} is reported in Ref. 5, we focus here on the gyro-moment expansion of $\Delta\mathcal{C}_{ab}^T$ and $\Delta\mathcal{C}_{ab}^F$, defined in Eqs. (57) and (58), respectively. First, we derive the Hermite-Laguerre projection of the test component of the correction term $\Delta\mathcal{C}_{ab}^{Tpj}$. As an initial step, we express $\bar{u}_{\parallel s}^k$ and $\bar{u}_{\perp s}^k$, defined in Eq. (34) and appearing in Eq. (33), in terms of the non-adiabatic gyro-moments n_a^{pj} . Injecting the expansion of h_a into $\bar{u}_{\parallel s}^k$ and $\bar{u}_{\perp s}^k$ yields

$$\bar{u}_{\parallel s}^k = v_{Ts} c_k \sum_{p=0}^{\infty} \sum_{j=0}^{\infty} n_a^{pj} I_{\parallel s}^{pj}, \quad (59a)$$

$$\bar{u}_{\perp s}^k = v_{Ts} c_k \sum_{p=0}^{\infty} \sum_{j=0}^{\infty} n_a^{pj} I_{\perp s}^{pj}, \quad (59b)$$

where we introduce the velocity integrals

$$I_{\parallel s}^{pj} = \frac{1}{N_a} \int d\mu dv_{\parallel} d\theta \frac{B}{m_a} \frac{H_p(s_{\parallel s}) L_j(x_s)}{\sqrt{2^p p!}} F_{Ms} L_k^{3/2}(s_s^2) J_{0s} s_{\parallel s} \quad (60)$$

and

$$I_{\perp s}^{pj} = \frac{1}{N_a} \int d\mu dv_{\parallel} d\theta \frac{B}{m_a} \frac{H_p(s_{\parallel s}) L_j(x_s)}{\sqrt{2^p p!}} F_{Ms} L_k^{3/2}(s_s^2) J_{1s} \sqrt{x_s}. \quad (61)$$

To analytically evaluate the velocity integrals in $I_{\parallel s}^{pj}$ and $I_{\perp s}^{pj}$, we expand the Bessel functions J_{0s} and J_{1s} in terms of associated Laguerre polynomials as follows³⁰,

$$J_m(b_s \sqrt{x_s}) = \left(\frac{b_s \sqrt{x_s}}{2} \right)^m \sum_{n=0}^{\infty} \frac{n! \mathcal{K}_n(b_s)}{(n+m)!} L_n^m(x_s), \quad (62)$$

with the n th-order kernel function $\mathcal{K}_n(b_s) = (b_s/2)^{2n} e^{-b_s^2/4}/n!$ describing FLR effects. Then, using Eq. (62) with

$$L_n^m(x) L_j(x) x^m = \sum_{s=0}^{n+m+j} d_{njs}^m L_s(x), \quad (63)$$

where closed analytical expressions for the coefficients d_{njs}^m are given in Ref. 5, the velocity integral in $I_{\parallel s}^{pj}$ can be computed,

$$I_{\parallel s}^{pj} = \frac{2}{3\sqrt{\pi}} \sum_{n=0}^{\infty} \sum_{f=0}^{n+j} (T^{-1})_{pf}^{1k0} \frac{\mathcal{K}_n(b_s)}{\sqrt{2^p p!}} d_{njf}^0 \frac{(k+3/2)!}{k!} \times [(p \geq 1 \cup f \geq 1) \cap (f + \lfloor p/2 \rfloor \geq k)], \quad (64)$$

with $[\cdot]$ the Iverson bracket ($[A] = 1$ if A is true, and 0 otherwise). Finally, the velocity integral contained in $I_{\perp s}^{pjk}$ can be evaluated similarly to the one in Eq. (64), and yields

$$I_{\perp s}^{pjk} = \sum_{n=0}^{\infty} \sum_{f=0}^{n+j+1} \sum_{r=0}^{f+\lfloor p/2 \rfloor} \sum_{q=0}^k \sum_{r_1=0}^r \frac{(T^{-1})_{pf}^{0r0}}{\sqrt{\pi}} \frac{b_s \mathcal{K}_n(b_s)}{(n+1)\sqrt{2^p p!}} \\ \times d_{njf}^1 L_{kq}^1 L_{rr_1}^0 (1/2 + r_1 + q)! . \quad (65)$$

We remark that the expression of the numerical coefficients $(T^{-1})_{pj}^{lkm}$ in Eqs. (64) and (65) can be found in Ref. 22, and arise from the basis transformation from Hermite-Laguerre to associated Legendre-Laguerre polynomials.

We now have all elements necessary to focus on the evaluation of $\Delta \mathcal{C}_{ab}^{Tpj}$ obtained by projecting Eq. (9) onto the Hermite-Laguerre basis. In Eq. (57), one recognises the quantities $I_{\parallel s}^{pjk}$ and $I_{\perp s}^{pjk}$ defined in Eqs. (64) and (65). Thus, using their definitions, the gyro-moment expansion of the test component of the correction terms, $\Delta \mathcal{C}_{ab}^{Tpj}$, is deduced

$$\Delta \mathcal{C}_{ab}^{Tpj} = \sum_{\ell=0}^L \sum_{k=0}^K \frac{2c_\ell}{\bar{\tau}_{ab}} \Delta M_{ab}^{\ell k} \left(\frac{\bar{u}_{\parallel a}^k}{v_{Ta}} I_{\parallel a}^{pj\ell} + \frac{\bar{u}_{\perp a}^k}{v_{Ta}} I_{\perp a}^{pj\ell} \right) . \quad (66)$$

We remark that $\Delta \mathcal{C}_{ab}^{Tpj}$ can then be expressed explicitly in terms of the non-adiabatic gyro-moments n_a^{lk} appearing in the definitions of $u_{\parallel a}^k$ and $u_{\perp a}^k$ given in Eq. (59).

Carrying out the same derivation yielding Eq. (66) for the gyro-moment expansion of the field component of the correction term, $\Delta \mathcal{C}_{ab}^{Fpj}$, defined in Eq. (58), and inverting the species role between a and b in $u_{\parallel s}^k$ and $u_{\perp s}^k$ yields

$$\Delta \mathcal{C}_{ab}^{Fpj} = \sum_{\ell=0}^L \sum_{k=0}^K \frac{2c_\ell}{\bar{\tau}_{ab}} \Delta N_{ab}^{\ell k} \left(\frac{\bar{u}_{\parallel b}^k}{v_{Ta}} I_{\parallel a}^{pj\ell} + \frac{\bar{u}_{\perp b}^k}{v_{Ta}} I_{\perp a}^{pj\ell} \right) , \quad (67)$$

where $\bar{u}_{\parallel b}^k$ and $\bar{u}_{\perp b}^k$ can be expressed in terms of the non-adiabatic gyro-moments of h_b by using Eq. (59). With the gyro-moment expansion of the test and field components of the correction term, given in Eqs. (66) and (67), the GK IS collision operator, Eq. (55), is expressed in terms of the non-adiabatic gyro-moments n_a^{pj} .

B. Expansion of the DK IS Collision Operator

We now consider the gyro-moment expansion of the GK IS collision operator, Eq. (55), in the DK limit. The gyro-moment expansion of the DK IS collision operator can be obtained by projecting Eq. (36) or by taking explicitly the zeroth-limit of the gyro-moment expansion of the GK IS collision operator Eq. (55). In both cases, it yields the following Hermite-Laguerre projections of the test and field components of the correction term,

$$\Delta\mathcal{C}_{ab}^{Tpj} = \sum_{\ell=0}^{\min(L,j+\lfloor p/2 \rfloor)} \sum_{k=0}^K \frac{(T^{-1})_{pj}^{1\ell}}{\sqrt{2^p} p!} \frac{(\ell+3/2)!}{\ell!} \frac{4c_\ell c_k}{3\sqrt{\pi}\bar{\tau}_{ab}} \Delta M_{ab}^{\ell k} \\ \times \mathbf{b} \cdot \mathbf{M}_a^{1k} [p \geq 1 \cup j \geq 1] \quad (68)$$

and

$$\Delta\mathcal{C}_{ab}^{Fpj} = \sum_{\ell=0}^{\min(L,j+\lfloor p/2 \rfloor)} \sum_{k=0}^K \frac{(T^{-1})_{pj}^{1\ell}}{\sqrt{2^p} p!} \frac{(\ell+3/2)!}{\ell!} \frac{4c_\ell c_k}{3\sqrt{\pi}\bar{\tau}_{ab}} \frac{1}{\chi} \Delta N_{ab}^{\ell k} \\ \mathbf{b} \cdot \mathbf{M}_b^{1k} [p \geq 1 \cup j \geq 1]. \quad (69)$$

In Eqs. (68) and (69), the spherical harmonic moments \mathbf{M}_a^{1k} , defined by Eq. (20) and related to the flow vectors in Eq. (24), are expressed as a function of the gyro-moments of the perturbed distribution function g_a , namely N_a^{pj} , by

$$\mathbf{b} \cdot \mathbf{M}_s^{1k} = \sum_{g=0}^{1+2k} \sum_{h=0}^k T_{1k}^{gh} \sqrt{2^g g!} N_s^{gh}, \quad (70)$$

where we use the fact that $f_a \simeq g_a$ in the DK limit. The basis transformation coefficients, T_{1k}^{gh} , are the DK basis transformation coefficients defined and derived in Ref. 29. With the gyro-moment expansion of the DK OS collision operator derived in Ref. 5, the DK IS collision operator follows by adding Eqs. (68) and (69) to the former.

VI. NUMERICAL TESTS AND COMPARISON BETWEEN COLLISION OPERATORS

Using the gyro-moment expansion of the IS collision operator, we perform the first numerical tests and comparisons between the IS, OS and the Coulomb collision operators. The discussion

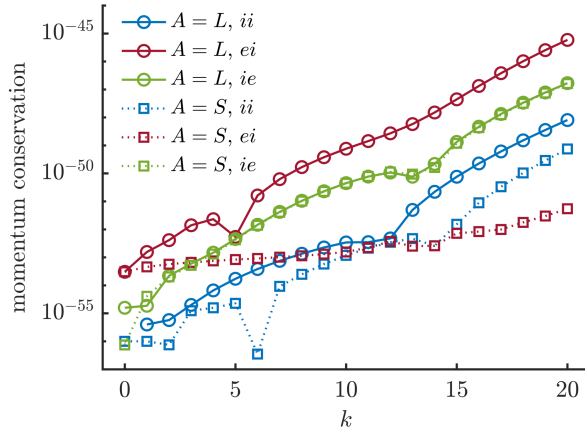


FIG. 1. Momentum conservation, Eq. (14), obtained using the closed expressions of the Braginskii matrices as a function of k for the Coulomb ($A = L$ and shown by the solid lines) and OS ($A = S$ and shown by the dotted lines) collision operators between electrons and ions with equal temperature $T_e = T_i$ and $m_e/m_i = 0.0027$.

of the numerical results is organized as follows. First, we discuss the numerical implementation of the closed analytical formulas appearing in the IS operator, in particular of the Braginskii matrices in Sec. VI A. We show that the numerical implementation satisfies the conservation laws and associated symmetry properties of Braginskii matrices to machine precision, regardless of the values of (L, J) . Then, as a first application of the IS collision operator using the gyro-moment approach, we investigate the collisionality dependence of TEM that develops at steep pressure gradients of the H-mode pedestal, and compare the IS with the OS and Coulomb collision operators in Sec. VI B. Finally, in Sec. VI C, we perform tests to study the collisional ZF damping and compare the numerical results with analytical predictions. The numerical tests show that the IS collision operator approaches better the Coulomb operator than the OS collision operator in the Pfirsch-Schlüter regime. In all cases investigated, $L = K \simeq 3$ terms in ΔC_{ab} are required for convergence.

A. Numerical Implementation

In the present work, the need of the numerical integration for the evaluation of the velocity integrals appearing in the definitions of $M_{ab}^{A\ell k}$ and $N_{ab}^{A\ell k}$ given in Eq. (13), as well as the velocity integrals involved in the gyro-moment expansion of the IS operator (see Eqs. (64) and (65)), is

Implementation of the Improved Sugama Collision Operator

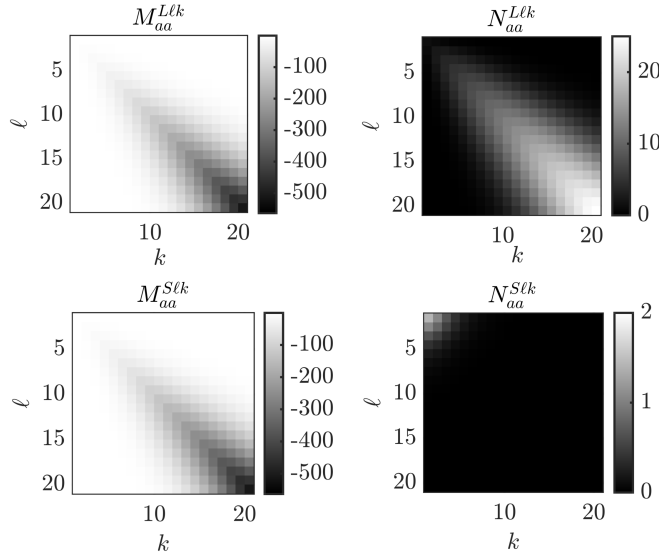


FIG. 2. Braginskii matrices of (top) Coulomb and (bottom) OS collision operators for like-species ($a = b$) associated with the test (left) and the field (right) components, respectively defined by $M_{aa}^{A\ell k}$ and $N_{aa}^{A\ell k}$, as a function of (ℓ, k) .

removed by using the closed analytical expressions given Sec. V. We note that the numerical error stemming from the numerical integration of the velocity integrals become arbitrarily large as the order of polynomials increases, and thus alter the accuracy of the Hermite-Laguerre projection for high-order gyro-moments. However, the evaluation of a large number of numerical coefficients is still required in the gyro-moment approach, which is affected by cancellation and round-off errors. Therefore, the analytical expressions in the present work are evaluated using an arbitrary-precision arithmetic software.

In Fig. 1, we display the momentum conservation, Eq. (14), as a function of k for both the Coulomb and OS collision operators. The momentum conservation law is satisfied within machine precision, illustrating the robustness of the numerical framework used in this work. Additionally, the Braginskii matrices, $M_{aa}^{A\ell k}$ and $N_{aa}^{A\ell k}$, of the Coulomb and OS collision operators are shown in Fig. 2 for the case of like-species collisions. Since the test components of both operators are equal in the case of like-species collisions, the Braginskii matrices $M_{aa}^{L\ell k}$ and $M_{aa}^{S\ell k}$ are equal, as shown in the left panel of Fig. 2. On the other hand, the difference in the Braginskii matrices associated with the field components, i.e. $N_{aa}^{A\ell k}$ (right panel of Fig. 2), arises due to the difference in the field component of the OS with respect to the Coulomb collision operator.

The gyro-moments approach allows us to investigate the coupling between gyro-moments in-

duced by the IS and OS collision operators. This can be done by truncating the Hermite-Laguerre expansion of h_a , see Eq. (51) (or g_a in the DK limit) at $(p, j) = (P, J)$ therefore, assuming that higher-order gyro-moments, $p > P$ and $j > J$, vanish. Given (P, J) , the gyro-moment expansion of the IS operator can be written as

$$\mathcal{C}_{ab}^{ISpj} = \sum_{p'=0}^P \sum_{j'=0}^J \mathcal{C}_{abp'j'}^{ISTpj} n_a^{p'j'} + \sum_{p'=0}^P \sum_{j'=0}^J \mathcal{C}_{abp'j'}^{ISFpj} n_b^{p'j'}. \quad (71)$$

An analogous expression can also be used for the OS collision operator. The coefficients $\mathcal{C}_{abp'j'}^{ISTpj}$ and $\mathcal{C}_{abp'j'}^{ISFpj}$ associated with the test and field components of \mathcal{C}_{ab}^{ISpj} can then be recast into a matrix form by using the one-dimensional index $\bar{l}(p, j) = (J+1)p + j + 1$, where (p, j) run from 0 to P and J , respectively. The matrices obtained from Eq. (71) allows us to illustrate the coupling between the gyro-moments associated with the GK IS and GK OS operators, as well as their difference for the case of like-species in Fig. 3. The same analysis is carried out for the DK operators in the same figure. We observe that, because of the self-adjoint relations of like-species collisions (see Eq. (4)), the gyro-moment matrices are symmetric. We also observe the block structure of the GK IS and OS, a consequence of vanishing polynomial basis coefficients $(T^{-1})_{pj}^{lkm}$. We remark that the analytical expressions of the lowest-order coefficients $\mathcal{C}_{abp'j'}^{ISTpj}$ and $\mathcal{C}_{abp'j'}^{ISFpj}$ associated with the DK IS, OS and Coulomb collision operators are reported in Appendix A.

B. Trapped electron Mode in Steep Pressure Gradient Conditions

The study of microinstabilities appearing in steep pressure gradient conditions have gained large interest in the past years because of their role in determining the turbulent transport in H-mode pedestals^{31–33}. The linear properties of mircroinstabilities at steep pressure gradients can significantly differ from the one at weaker gradients, typically found in the core. For example, unconventional ballooning mode structures can be encountered if the pressure gradients are above a certain linear threshold with the location of the largest mode amplitude being shifted from the outboard midplane position, in contrast to the conventional mode structure found at lower gradients^{34,35}. Because the pedestal is characterized by a wide range of collisionalities ranging from the low-collisionality banana (at the top of the pedestal) to the high-collisionality Pfisch-Schlüter regime (at the bottom of the pedestal and in the SOL)³⁶, an accurate collision operator is

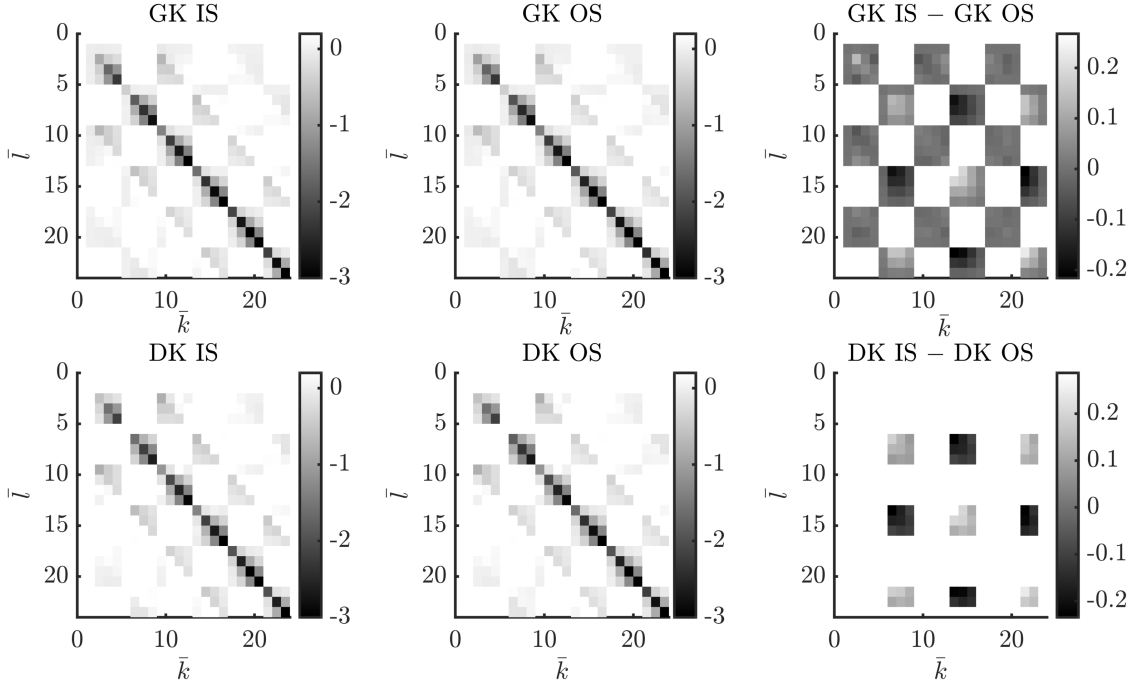


FIG. 3. Gyro-moment matrices of the IS (left), OS (center) and their relative difference (right), given by the gyro-moment expansion of the correction term ΔC_{ab} (see Sec. V). Both the GK (top) and DK (bottom) limits for the IS and OS operator are shown. Here, we consider $k_\perp = 0.5$ and $(P, J) = (6, 3)$ gyro-moments, with $L = K = 5$ in the IS collision operator.

necessary for the proper description and interaction of these modes. Thus, we compare the properties of steep pressure gradient TEM, when the IS, the OS and the Coulomb collision operators are used.

To carry out this numerical investigation, a linear flux-tube code using the gyro-moment approach has been implemented to solve the electromagnetic GK Boltzmann equation. While a detailed description of this code will be the subject to a future publication, here we mention that we assume concentric, circular and closed magnetic flux surfaces using the $s - \alpha$ model (with $\alpha = 0$)³⁷. In the local flux-tube approach, we assume constant radial density and temperature gradients, L_N^{-1} and L_{Ta}^{-1} , with values $R_0/L_N = R_0/L_{Ti} = R_0/L_{Te} = 20$, where R_0 is the tokamak major radius. Electromagnetic effects are introduced with $\beta_e = 8\pi P_e^2/B_0^2 = 0.01\%$. For numerical reasons, we use a reduced ion mass $m_e/m_i = 0.0027$. The local safety factor q , the magnetic shear s and the inverse aspect ratio ϵ are fixed at $q = 2.7$, $s = 0.5$ and $\epsilon = 0.18$. Additionally, we center the k_x spectrum around $k_x = 0$. Collisional effects are introduced by using the gyro-moment

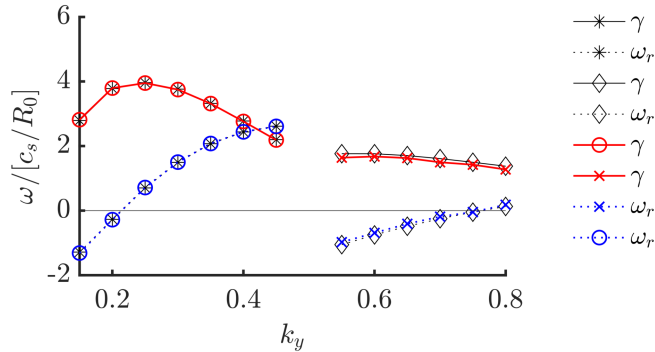


FIG. 4. Collisionless growth rate γ (red lines) and frequency ω_r (blue lines) as a function of the binormal wavenumber k_y plotted on the same axis. The colored lines are the results obtained by the gyro-moment approach using $(P, J) = (20, 10)$ and the black markers are the collisionless results using the GENE eigen-solver. A positive mode frequency, $\omega_r > 0$, corresponds to the mode propagating in the ion diamagnetic direction and a negative mode frequency, $\omega_r < 0$, to the electron diamagnetic direction. Here, $T_i/T_e = 1$.

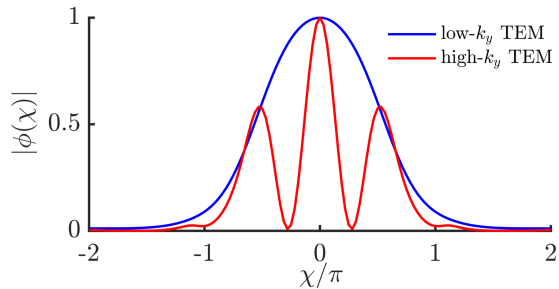


FIG. 5. Modulus of the electrostatic ballooning eigenmode function, $\phi(\chi)$ (normalized to $\phi(\chi = 0)$), as a function of the ballooning angle χ corresponding to the case of the low- k_y TEM at $k_y = 0.25$ (blue solid line) and to the high- k_y TEM developing at $k_y = 0.6$ (red solid line).

expansion of the IS operator derived in this work and the ones reported in Ref. 5.

Given these parameters, we identify two branches of unstable modes developing at different values of the binormal wavenumber k_y in the collisionless limit. This is shown in Fig. 4 where the growth rate γ and the real mode frequency ω_r are plotted as a function of k_y using $(P, J) = (20, 10)$ gyro-moments. We remark that the collisionless GENE simulations are in excellent agreement with the gyro-moment approach, verifying its validity in collisionless H-mode conditions. A frequency jump from positive to negative values indicates a mode transition. While the mode peaking at $k_y = 0.25$ (k_y is normalized to the ion sound Larmor radius) is normally identified as the ITG

Implementation of the Improved Sugama Collision Operator

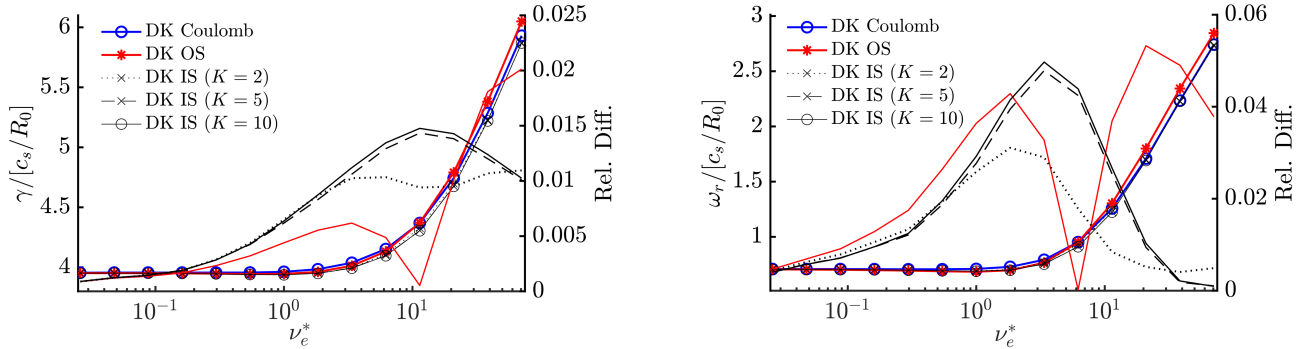
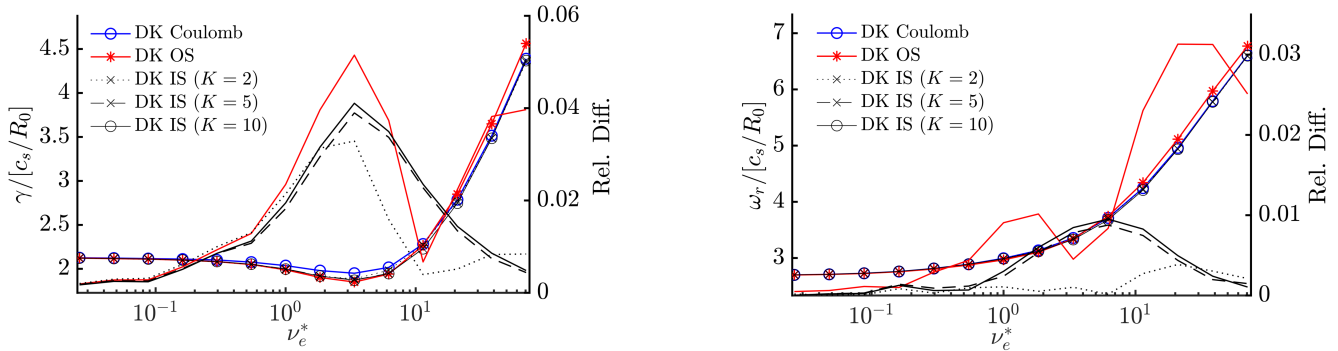


FIG. 6. The low- k_y TEM growth rate γ (left) and mode frequency ω_r (right) as a function of v_e^* . The different DK collision operators considered are the DK Coulomb (blue circle), the DK OS (red stars), the DK IS with $K = 2$ (dotted black cross), the DK IS with $K = 5$ (dashed-dotted black cross) and the DK IS with $K = 10$ collision operators (solid black circle). The relative differences of each operator relative to the DK Coulomb are plotted by the lines without markers. The lines with and without markers are plotted with respect to the left and right y-axis, respectively. Here, the parameters are the same as in Fig. 4 at $k_y = 0.25$ with $T_i/T_e = 1$.

mode at lower gradients because of its propagation along the ion diamagnetic direction ($\omega_r > 0$), we identify it here as a TEM with a conventional mode structure. Indeed, despite $\omega_r > 0$, the mode persists if the ion and electron temperature gradients are removed from the system, while it is stabilised if the electrons are assumed adiabatic. The discontinuity observed in Fig. 4 is due to a transition to a TEM developing at $k_y \gtrsim 0.5$ with an unconventional ballooning mode structures with secondary peaks located near $\chi = \pm\pi/2$ (χ is the ballooning angle) away from the outboard midplane (where the mode at $k_y \sim 0.2$ peaks), as shown in Fig. 5. Hence, we refer to the TEM peaking at $k_y = 0.25$, with a conventional mode structure, as the low- k_y TEM and to the TEM peaking near $k_y = 0.6$, with an unconventional mode structure, as the high- k_y TEM. We also notice that the low- k_y TEM and the high- k_y TEM change continuously from electron to the ion diamagnetic directions as k_y increases³⁸.

We now investigate the collisionality dependence of both modes. While the electron collisionality is expected to be mainly in the banana regime with $v_e^* = \sqrt{2}qv/\varepsilon^{3/2} \lesssim 1$ in the middle of the pedestal of present and future tokamak devices (with v the ion-ion collision frequency normalized to c_s/R_0 , see Ref. 5), the temperature drop yields collisionalities in the Pfirsch-Schlüter regime, $v_e^* \sim 1/\varepsilon^{3/2} \gg 1$, at the bottom of the pedestal³⁶. Focusing first on the low- k_y TEM ($k_y = 0.25$), we


 FIG. 7. Same as Fig. 6 but with $T_i/T_e = 2$.

notice that since it develops at low binormal wavenumber, the DK limits of the collision operators are considered (numerical tests show that FLR effects at $k_y = 0.25$ change the value of the growth rate γ by less than 1% at the level of collisionalities explored). The growth rate and the real mode frequency obtained by using the DK Coulomb, DK OS and DK IS using $K = 2, 5$ and 10 terms in Eq. (36) are shown as a function of ν_e^* in Fig. 6. In addition, the relative difference of the IS and OS operators with respect to the DK Coulomb is computed and displayed. Numerical tests show that our results are converged by evolving $(P, J) = (20, 10)$ gyro-moments (as in Fig. 4) and that a smaller number of gyro-moments is actually sufficient in the Pfirsch-Schlüter regime⁵. It is first observed that the low- k_y TEM is destabilized by collisions in the Pfirsh-Schlüter regime, where both the growth rate and frequency increase with collisionality. In addition, while the deviation between the DK OS and DK Coulomb increases with ν_e^* , the DK IS is able to correct the DK OS and to approach the DK Coulomb as L and K increase. More precisely, while the relative difference between the DK OS and DK Coulomb operators is of the order of 2%, the use of the DK IS decreases this difference to less than 1% in the case $L = K = 5$. While a small difference remains in the growth rate at high collisionality between the Coulomb and DK IS operators, the mode frequency ω_r of the DK Coulomb is well reproduced by the DK IS with $L = K \gtrsim 3$ in Eq. (36), parameters that therefore ensure a good convergence of the DK IS.

The deviations between the OS and DK Coulomb depend on the temperature ratio of the colliding species (as well as on the mass ratio). In order to study the impact of the ion to electron temperature ratio, we consider the case $T_i/T_e = 2$ as shown in Fig. 7 (the other parameters are the same as in Fig. 6). We observe that the relative differences of the growth rate and of the mode frequency between the Coulomb and OS operator increase with T_i/T_e . However, the DK IS reduces

Implementation of the Improved Sugama Collision Operator

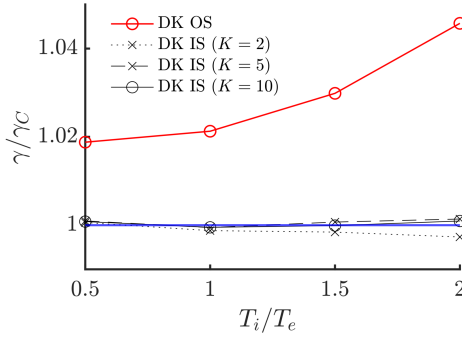


FIG. 8. Ratio γ/γ_C between the growth rate, γ , predicted by the OS (red lines) and IS (black lines) with $K = 2$, $K = 5$ and $K = 10$ operators and the growth rate, γ_C , obtained using the Coulomb collision operator, as a function T_i/T_e . The same parameters as in Fig. 6 are used, except for $v_e^* = 50$.

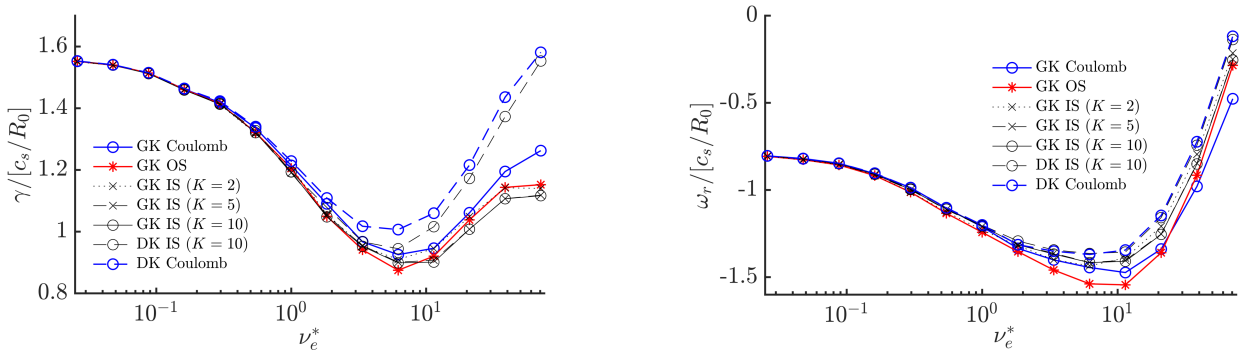


FIG. 9. Shown is the high- k_y TEM growth rate γ (left) and the real mode frequency ω_r (right) as a function of v_e^* . The results obtained with the GK Coulomb (blue solid line), the GK OS (red solid line), the GK IS with $K = 3$ (dotted black lines), the GK IS with $K = 5$ (dashed black lines with cross) and the GK IS with $K = 10$ collision operators (solid black lines) are plotted with the predictions of the DK IS with $K = 10$ (dashed black lines with circles) and the DK Coulomb operators (dashed blue lines with circles). Here, the parameters are the same as in Fig. 4 at $k_y = 0.6$ with $T_i/T_e = 1$.

this difference to less than 1% when $T_i/T_e = 2$. This can be better represented by considering the ratio between the growth rate γ , predicted by the IS and OS operators, and γ_C , obtained using the Coulomb operator, plotted as a function of the temperature ratio T_i/T_e and shown in Fig. 8. The correction terms enable the IS operator to better approximate the Coulomb collision operator in the Pfirsch-Schlüter regime than the OS operator when $v_e^* = 50$ as T_i/T_e increases.

We now turn to the collisionality dependence of the high- k_y TEM mode developing near $k_y =$

0.6 (see Fig. 4). As the perpendicular wavenumber in the argument of the Bessel functions increases, a large number of terms in the infinite sums arising from the expansion of the Bessel functions, Eq. (62), is required for convergence. We evaluate the GK collision operators by truncating the infinite sums in $I_{\parallel s}^{pjk}$ and $I_{\perp s}^{pjk}$, defined in Eqs. (64) and (65), at $n = 6$ (we have verified that our results are converged). The high- k_y TEM growth rate γ and mode frequency ω_r obtained by using the same parameters in Fig. 4 (for $k_y = 0.6$) are shown in Fig. 9, as a function of the electron collisionality v_e^* . We consider the GK Coulomb, GK OS and GK IS with different values of $L = K$, as well as the DK IS (with $L = K = 10$) and DK Coulomb collision operators. First, we observe that the TEM is stabilized by collisional effects because of the FLR terms present in the GK IS collision operators for all values of K , as revealed by the comparison with the DK IS (with $K = 10$) and the DK Coulomb collision operators. Second, the GK IS yields a smaller growth rate and higher mode frequency in the Pfirsch-Schlüter regime than the GK OS. Third, in the high-collisional regime, the GK IS and OS both yield a stronger damping than the GK Coulomb. This difference, which is enhanced as both the collisionality and k_y increase, stems mainly from the approximation in Eq. (35) used for the former operators. Finally, we remark that, consistently with the previous case, convergence of the GK IS operator is achieved when $L = K \gtrsim 3$. Overall, the GK IS and GK OS yield a similar collisionality dependence of the high- k_y TEM, with a difference in the growth rate $\lesssim 10\%$. While only the case $T_i = T_e$ is shown in Fig. 9, this holds also in the $T_e \neq T_i$ case.

C. Collisional Zonal Flow Damping

Axisymmetric, poloidal zonal flows (ZFs) are believed to be among the key physical mechanisms at play in the L-H mode transition⁴⁰ by, ultimately, regulating the level of turbulent transport. It is therefore of primary importance to test and compare the effect of collisions, modelled by using the IS, OS and Coulomb collision operators, on their dynamics.

While the collisionless damping to a residual level of the ZFs has been originally addressed in Ref. 39, the collisional ZF damping has been studied in Ref. 41 in the banana regime when $v_i^* \lesssim 1$ (with v_i^* the ion-ion collisionality) for radial wavelengths much longer than the ion poloidal gyroradius, assuming adiabatic electrons, and using a pitch-angle scattering operator mimicking the collisional drag of energetic ions. A refinement of the exponential decay in Ref. 41 of the ZF residual prediction $R_z(\infty) = \phi_z(\infty)/\phi_z(0)$ (with $\phi_z(t)$ the flux-surface averaged potential) with

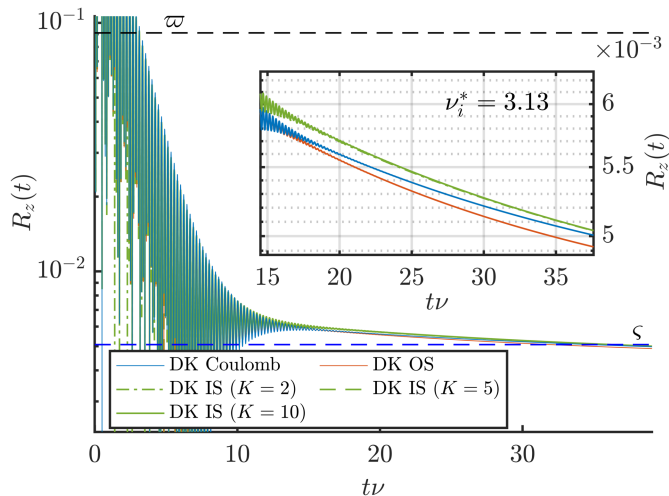


FIG. 10. Collisional ZF damping obtained using the DK Coulomb (blue solid line), DK OS (red solid line) and DK IS with $L = K = 2, 5, 10$ (green lines) collision operators in the Pfirsch-Shlüter regime $\nu_i^* = 3.13$. The collisionless (see Ref. 39) and collisional (see Eq. (72)) long time predictions, $\bar{\omega} = 1/(1 + 1.6q/\sqrt{\epsilon})$ and ζ , are plotted by the dashed black and blue lines, respectively. Here, $k_x = 0.05$, $q = 1.4$ and $\epsilon = 0.1$.

a momentum restoring pitch-angle scattering operator was later derived in Ref. 42 for long wavelength modes,

$$R_z(\infty) \rightarrow \zeta = \frac{\epsilon^2}{q^2} \frac{1}{(1 + \epsilon^2/q^2)}. \quad (72)$$

Even if Eq. (72) does not include energy diffusion as well as the effects of GK terms in the collision operator, it still provides a good estimate asymptotic ZF residual predicted by the DK IS, as shown below.

For our tests, we consider only ion-ion collisions and, by including the IS operator, we extend the study of Ref. 5, where the differences between the GK OS and GK Coulomb operators in the collisional ZF damping are illustrated, finding a stronger damping by the former. We focus on the Pfirsch-Schlüter regime with $\nu_i^* = 3.13$, with convergence being achieved with $(P, J) = (24, 10)$ gyro-moments. The collisional time traces of the ZF residual, $R_z(t) = \phi_z(t)/\phi_z(0)$, obtained for the DK IS (with $K = L = 2, 5, 10$), DK OS and DK Coulomb collision operators are shown in Fig. 10 for $k_x = 0.05$ and in Fig. 11 for the $k_x = 0.1$ and $k_x = 0.2$ using the GK operators. Starting from the case of small radial wavenumber $k_x = 0.05$, we first observe that all DK operators agree

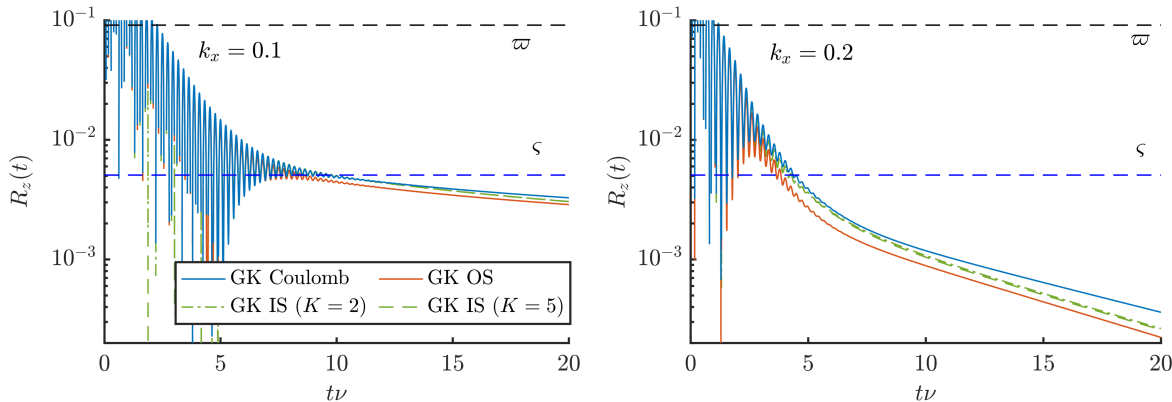


FIG. 11. Collisional ZF damping obtained using the GK Coulomb (blue lines), GK OS (red solid lines) and GK IS (green lines) collision operators with $K = 2$ (dashed-dotted lines) and $K = 5$ (dashed lines). The damping of an initial density perturbation with a radial wavenumber $k_x = 0.1$ (left) and $k_x = 0.2$ (right) are shown. The analytical collisionless and collisional predictions, ϖ and ζ , are plotted for comparison. It is observed that the GK IS collision operator provides better approximation to the GK Coulomb operator. The parameters and the number of gyro-moments are the same as in Fig. 10.

with the analytical long time prediction given in Eq. (72), despite the absence of energy diffusion in the latter. Consistently with Ref. 5, the DK Sugama yields a stronger damping of the ZF than the DK Coulomb. The addition of the correction terms to the OS operator allows the DK IS to better approximate the DK Coulomb operator, yielding a weaker damping of the ZF. We remark that only a small difference between the $L = K = 2, 5$ cases is noticeable showing that $L = K \simeq 3$ is necessary for the DK IS to converge also in this case.

We now consider the collisional ZF damping at larger k_x values using the GK IS, GK OS and GK Coulomb collision operators, $k_x = 0.1$ and $k_x = 0.2$, and plot the results in Fig. 11. The same collisionality of the $k_x = 0.05$ case is used. Only the $K = 2, 5$ cases are considered for the GK IS for simplicity, since convergence is achieved with these parameters. First, consistently with Ref. 5, it is observed that the GK OS produces a stronger ZF damping with respect to the GK Coulomb. Second, the GK IS collision operator provides a better approximation to the GK Coulomb collision operator than the GK OS operator. This is particularly true in the early phase of the damping i.e. $t\nu \lesssim 10$. Although the GK IS still yields a better approximation than the GK OS, larger GK IS departures from the GK Coulomb are observed at later times when the GAM oscillations are completely suppressed. For larger collisionalities and smaller scale lengths, the same observations

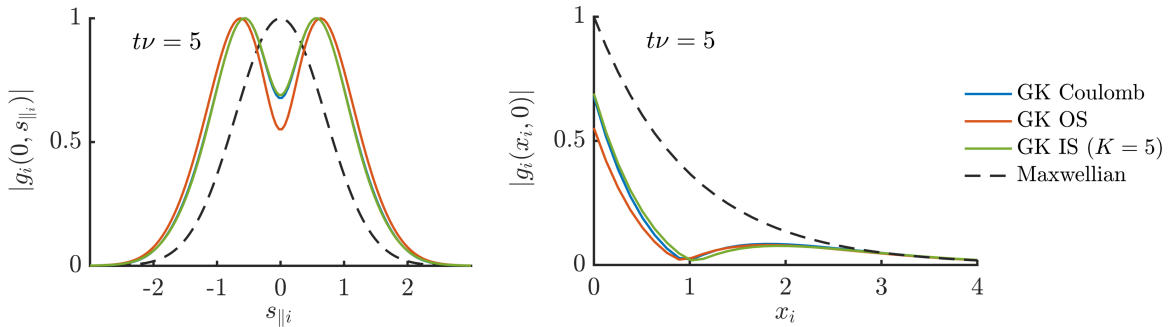


FIG. 12. Modulus of the perturbed ion gyrocenter distribution function $|g_i|$ (normalized to its maximum value), at time $t\nu = 5$ after the damping of the GAM oscillations and at the outboard midplane in Fig. 11, plotted as a function of $s_{\parallel i}$ at $x_i = 0$ (left) and as a function of x_i at $s_{\parallel i} = 0$ (right). The case of a Maxwellian distribution function $e^{-s_{\parallel i}^2 - x_i}$ is shown for comparison (dashed black lines).

about the rapid ZF decay made at lower collisionalities hold.

Finally, we investigate the effects of the GK collision operators on the ion velocity-space distribution function. We consider the modulus of the perturbed ion distribution function, $|g_i|$, obtained by using Eq. (51), at time $t\nu = 5$ after the damping of the GAM oscillations, for the case $k_x = 0.2$. We plot $|g_i|$ as a function of $s_{\parallel i}$ (at $x_i = 0$) and x_i (at $s_{\parallel i} = 0$) in Fig. 12, respectively, for the different GK collision operators. It is observed that the GK IS yields similar velocity-space structures along both the parallel and perpendicular directions than the GK OS operator with the distribution function being depleted in the region of the velocity-space $|v_{\parallel}| \lesssim v_{Ti}$ more strongly than the GK Coulomb operator. A similar observation can be made when $v_{\perp} \lesssim v_{Ti}$, as shown in the right panel of Fig. 12.

VII. CONCLUSION

In this work, the gyro-moment method has been applied to implement the recently developed GK improved Sugama (IS) collision operator¹⁷. Designed to extend the validity of the original Sugama (OS) collision operator to the Pfirsch-Schlüter regime, the Hermite-Laguerre expansion of the perturbed distribution function allows expressing the IS collision operator as a linear combination of gyro-moments, with coefficients that are analytical functions of the mass and temperature ratios of the colliding species and, in the GK limit, perpendicular wavenumber. In particular, analytical expressions of the Braginskii matrices, $M_{ab}^{A\ell k}$ and $N_a^{A\ell k}$, associated with the Coulomb and

Implementation of the Improved Sugama Collision Operator

OS collision operators are obtained for arbitrary (ℓ, k) using the spherical harmonic expansion⁵. This allows the evaluations of the correction terms that are added to the OS operator yielding the IS collision operators for arbitrary gyro-moments.

We describe the numerical implementation of the IS collision operator. This is based on an arbitrary precision arithmetic library to avoid the numerical loss of precision and round-off errors when evaluating the Braginskii matrices. We demonstrated that the conservation laws (particle, momentum, and energy) are satisfied at arbitrary order in (ℓ, k) . The IS collision operator is tested and compared with the OS and Coulomb collision operator in edge conditions at steep pressure gradients and high collisionality. Two test cases are considered, that involve the evaluation of the TEM growth rate and frequency at steep gradients and the damping of ZF. The analysis of the linear properties of a conventional TEM, developing at long wavelengths, reveals that the IS is able to approximate the TEM growth rate and frequency predicted by the DK Coulomb operator better than the OS, particularly in the Pfirsch-Schlüter regime. At small perpendicular wavelengths and high-collisionality, the study an unconventional TEM shows that the GK IS and GK OS essentially yields to the same FLR damping, within a 10% of difference. The collisional ZF damping is also explored and compared with analytical results. The analysis shows that the IS operator yields an intermediate value of the ZF residual, between the weaker value produced by the OS operator and the larger ZF residual predicted by the Coulomb collision operator. Despite the fact that the IS and OS produce linear results that differ by less than 10% in all cases explored in the present work, nonlinear turbulent simulations are still required to investigate the impact of this difference on the saturated turbulent state when the collisionality is high.

The computational cost of the gyro-moment approach is reduced as the collisionality increases. This offers an ideal framework to construct reduced fluid-like models to explore turbulent transport in the boundary of fusion devices. As an example, the analytical expression derived in this work allow us to evaluate the lowest-order gyro-moment terms of the IS, OS and Coulomb collision operators in App. A. Finally, we remark that the expressions presented in this work can be easily extended to the study of multicomponent plasmas with species of different mass and temperature.

ACKNOWLEDGEMENT

This work has been carried out within the framework of the EUROfusion Consortium, funded by the European Union via the Euratom Research and Training Programme (Grant Agreement No

101052200 — EUROfusion). Views and opinions expressed are however those of the author(s) only and do not necessarily reflect those of the European Union or the European Commission. Neither the European Union nor the European Commission can be held responsible for them. The simulations presented herein were carried out in part on the CINECA Marconi supercomputer under the TSVVT421 project and in part at CSCS (Swiss National Supercomputing Center). This work was supported in part by the Swiss National Science Foundation.

Appendix A: Lowest-Order Gyro-Moment Analytical Expressions

At high-collisionality, the number of gyro-moments necessary to describe the perturbed distribution function g_a is reduced since higher-order gyro-moments are strongly damped by collisions. In this regime, the perturbed distribution function is well approximated by a perturbed Maxwellian, with its perturbation that has a relative amplitude of the order of the ratio of the particle mean-free path to the typical parallel scale length, i.e. $\lambda_{mfp}/L_{\parallel} \ll 1$. The Maxwellian gyro-moments (p, j) , i.e. the gyrocenter density $(0, 0)$, the parallel gyrocenter velocity $(1, 0)$, the parallel and perpendicular temperatures, $(2, 0)$ and $(0, 1)$ respectively are leading order in $\lambda_{mfp}/L_{\parallel}$. On the other hand, the gyro-moments, associated with the non-Maxwellian component of g_a , i.e. the parallel and perpendicular heat fluxes $(3, 0)$ and $(1, 1)$, respectively are first order in $\lambda_{mfp}/L_{\parallel}$.

By projecting the GK Boltzmann equation on the Hermite-Laguerre basis²¹, the gyro-moment expansion of the IS collision operator, presented in this work, allows us to evaluate explicitly the collisional terms that enter in the evolution equations of the lowest-order gyro-moment enumerated above. We consider the DK IS collision operator (FLR effects yield complicated coefficients that rely on sums with the number of significant terms that depends on k_{\perp}). Using the closed analytical formulas of the DK IS, given in Eqs. (68) and (69), the non-vanishing terms $\Delta\mathcal{C}_{abp'j'}^{Tpj}$ in the gyro-moment expansion of the test component $\Delta\mathcal{C}_{ab}^{Tpj}$ (see Eq. (71)), are given by

$$\Delta \mathcal{C}_{ab30}^{T10} = \frac{4\tau^{3/2} v_{ab}}{5(\sigma + \tau)^{5/2}} \sqrt{\frac{6}{\pi}} \left[\tau \left(-\sqrt{\frac{(\sigma + 1)\tau}{\sigma + \tau}} + \sigma + 1 \right) - \sigma \sqrt{\frac{(\sigma + 1)\tau}{\sigma + \tau}} \right], \quad (\text{A1a})$$

$$\Delta \mathcal{C}_{ab11}^{T10} = \frac{8\tau^{3/2} v_{ab}}{5\sqrt{\pi}(\sigma + \tau)^{5/2}} \left[\sigma \sqrt{\frac{(\sigma + 1)\tau}{\sigma + \tau}} + \tau \left(\sqrt{\frac{(\sigma + 1)\tau}{\sigma + \tau}} - \sigma - 1 \right) \right], \quad (\text{A1b})$$

$$\Delta \mathcal{C}_{ab10}^{T30} = -\frac{4\sqrt{\tau} v_{ab}}{5(\sigma + \tau)^{5/2}} \sqrt{\frac{2}{3\pi}} \left[10\sigma^2(\tau - 1) + 3\sqrt{\frac{(\sigma + 1)\tau^5}{\sigma + \tau}} + \sigma\tau \left(3\sqrt{\frac{(\sigma + 1)\tau}{\sigma + \tau}} + \tau - 4 \right) - 3\tau^2 \right], \quad (\text{A1c})$$

$$\Delta \mathcal{C}_{ab30}^{T30} = -\frac{12v_{ab}\sigma(\tau - 1)\sqrt{\tau}(10\sigma^2 - 2\sigma\tau + 3\tau^2)}{25\sqrt{\pi}(\sigma + \tau)^{7/2}}, \quad (\text{A1d})$$

$$\Delta \mathcal{C}_{ab11}^{T30} = \frac{4v_{ab}\sqrt{\frac{6}{\pi}}\sigma(\tau - 1)\sqrt{\tau}(10\sigma^2 - 2\sigma\tau + 3\tau^2)}{25(\sigma + \tau)^{7/2}}, \quad (\text{A1e})$$

$$\Delta \mathcal{C}_{ab10}^{T11} = \frac{8v_{ab}\sqrt{\tau}}{15\sqrt{\pi}(\sigma + \tau)^{5/2}} \left[10\sigma^2(\tau - 1) + 3\sqrt{\frac{(\sigma + 1)\tau^5}{\sigma + \tau}} + \sigma\tau \left(3\sqrt{\frac{(\sigma + 1)\tau}{\sigma + \tau}} + \tau - 4 \right) - 3\tau^2 \right], \quad (\text{A1f})$$

$$\Delta \mathcal{C}_{ab30}^{T11} = \Delta \mathcal{C}_{ab11}^{T30}, \quad (\text{A1g})$$

$$\Delta \mathcal{C}_{ab11}^{T11} = -\frac{8v_{ab}\sigma(\tau - 1)\sqrt{\tau}(10\sigma^2 - 2\sigma\tau + 3\tau^2)}{25\sqrt{\pi}(\sigma + \tau)^{7/2}}, \quad (\text{A1h})$$

where $\tau = T_a/T_b$, $\sigma = m_a/m_b$ are the temperature and mass ratios of the colliding species, respectively. Similarly, the non-vanishing terms $\Delta \mathcal{C}_{ab,p'j'}^{Tpj}$ in the gyro-moment expansion of the field component $\Delta \mathcal{C}_{ab}^{Fpj}$ (see Eq. (71)) are

$$\Delta \mathcal{C}_{ab30}^{F10} = -\frac{4\sqrt{\frac{6}{\pi}}\sigma^{3/2}\tau\left(-\sqrt{(\sigma+1)(\sigma+\tau)}+\sigma+1\right)}{5(\sigma+\tau)^{5/2}}, \quad (\text{A2a})$$

$$\Delta \mathcal{C}_{ab11}^{F10} = \frac{8\sigma\sqrt{\sigma\tau}\left(-\sqrt{(\sigma+1)\tau^3}+\sigma\left(\sqrt{\tau(\sigma+\tau)}-\sqrt{(\sigma+1)\tau}\right)+\sqrt{\tau(\sigma+\tau)}\right)}{5\sqrt{\pi}(\sigma+\tau)^3}, \quad (\text{A2b})$$

$$\Delta \mathcal{C}_{ab10}^{F30} = \frac{4\sqrt{\frac{6}{\pi}}\sqrt{\sigma}\tau\left(\sqrt{(\sigma+1)\tau^3}+\tau\left(-\sqrt{\sigma+\tau}\right)+\sigma\left(-3\tau\sqrt{\sigma+\tau}+\sqrt{(\sigma+1)\tau}+2\sqrt{\sigma+\tau}\right)\right)}{5(\sigma+\tau)^3}, \quad (\text{A2c})$$

$$\Delta \mathcal{C}_{ab30}^{F30} = \frac{36\sigma^{3/2}\tau\left(\sigma\left(5\tau-\sqrt{\tau}-2\right)-\left(\sqrt{\tau}-3\right)\tau\right)}{25\sqrt{\pi}(\sigma+\tau)^{7/2}}, \quad (\text{A2d})$$

$$\Delta \mathcal{C}_{ab11}^{F30} = \frac{12\sqrt{\frac{6}{\pi}}\sigma^{3/2}\tau\left(\sigma\left(-5\tau+\sqrt{\tau}+2\right)+\left(\sqrt{\tau}-3\right)\tau\right)}{25(\sigma+\tau)^{7/2}}, \quad (\text{A2e})$$

$$\Delta \mathcal{C}_{ab10}^{F11} = -\frac{8\sqrt{\sigma\tau}\left(\sigma\left(-3\sqrt{\tau^3(\sigma+\tau)}+\sqrt{\sigma+1}\tau+2\sqrt{\tau(\sigma+\tau)}\right)-\sqrt{\tau^3(\sigma+\tau)}+\sqrt{\sigma+1}\tau^2\right)}{5\sqrt{\pi}(\sigma+\tau)^3}, \quad (\text{A2f})$$

$$\Delta \mathcal{C}_{ab30}^{F11} = \Delta \mathcal{C}_{ab11}^{F30}, \quad (\text{A2g})$$

$$\Delta \mathcal{C}_{ab11}^{F11} = \frac{24\sigma^{3/2}\tau\left(\sigma\left(5\tau-\sqrt{\tau}-2\right)-\left(\sqrt{\tau}-3\right)\tau\right)}{25\sqrt{\pi}(\sigma+\tau)^{7/2}}. \quad (\text{A2h})$$

We notice that, from the conservation of particle in Eq. (2a), it follows $\Delta \mathcal{C}_{ab,p'j'}^{T00} = \Delta \mathcal{C}_{ab,p'j'}^{F00}$. We also provide the non-vanishing lowest-order terms in the gyro-moment expansion of the OS collision operator, that are given by

$$\mathcal{C}_{ab10}^{ST10} = -\frac{8v_{ab}(\sigma+1)}{3\sqrt{\pi}} \left(\frac{\tau}{\sigma+\tau} \right)^{3/2}, \quad (\text{A3a})$$

$$\mathcal{C}_{ab30}^{ST10} = \frac{4v_{ab}}{5} \sqrt{\frac{6}{\pi}} \frac{\sqrt{\sigma+1}\tau^2}{(\sigma+\tau)^2}, \quad (\text{A3b})$$

$$\mathcal{C}_{ab11}^{ST10} = -\frac{8v_{ab}\sqrt{\sigma+1}\tau^2}{5\sqrt{\pi}(\sigma+\tau)^2}, \quad (\text{A3c})$$

$$\mathcal{C}_{ab20}^{ST20} = -\frac{16v_{ab}\sqrt{\tau}(5\sigma^2(\tau+2)+21\sigma\tau+6\tau^2)}{45\sqrt{\pi}(\sigma+\tau)^{5/2}}, \quad (\text{A3d})$$

$$\mathcal{C}_{ab01}^{ST20} = -\frac{16v_{ab}\sqrt{\frac{2}{\pi}}\sqrt{\tau}(-5\sigma^2(\tau-1)+3\sigma\tau+3\tau^2)}{45(\sigma+\tau)^{5/2}}, \quad (\text{A3e})$$

$$\mathcal{C}_{ab01}^{ST01} = -\frac{16v_{ab}\sqrt{\tau}(5\sigma^2+2(5\sigma+9)\sigma\tau+3\tau^2)}{45\sqrt{\pi}(\sigma+\tau)^{5/2}}, \quad (\text{A3f})$$

$$\mathcal{C}_{ab30}^{ST30} = -\frac{4v_{ab}\sqrt{\tau}(70\sigma^2+56\sigma\tau+31\tau^2)}{35\sqrt{\pi}(\sigma+\tau)^{5/2}}, \quad (\text{A3g})$$

$$\mathcal{C}_{ab11}^{ST30} = -\frac{4v_{ab}\sqrt{\frac{2}{3\pi}}\tau^{3/2}(28\sigma+\tau)}{35(\sigma+\tau)^{5/2}}, \quad (\text{A3h})$$

$$\mathcal{C}_{ab11}^{ST11} = -\frac{8v_{ab}\sqrt{\tau}(105\sigma^2+98\sigma\tau+47\tau^2)}{105\sqrt{\pi}(\sigma+\tau)^{5/2}}, \quad (\text{A3i})$$

with $\mathcal{C}_{ablk}^{STpj} = \mathcal{C}_{abpj}^{STlk}$, and

$$\mathcal{C}_{ab10}^{SF10} = \frac{8v_{ab}\sigma(\sigma+1)\tau}{3\sqrt{\pi}\sqrt{\sigma(\sigma+\tau)^3}}, \quad (\text{A4a})$$

$$\mathcal{C}_{ab30}^{SF10} = -\frac{4v_{ab}\sqrt{\frac{6}{\pi}}\sqrt{\sigma^3(\sigma+1)}\tau}{5(\sigma+\tau)^2}, \quad (\text{A4b})$$

$$\mathcal{C}_{ab11}^{SF10} = \frac{8v_{ab}\sqrt{\sigma^3(\sigma+1)}\tau}{5\sqrt{\pi}(\sigma+\tau)^2}, \quad (\text{A4c})$$

$$\mathcal{C}_{ab20}^{SF20} = \frac{16v_{ab}\sigma(\sigma+1)\tau^{3/2}}{9\sqrt{\pi}(\sigma+\tau)^{5/2}}, \quad (\text{A4d})$$

$$\mathcal{C}_{ab01}^{SF20} = -\frac{16v_{ab}\sqrt{\frac{2}{\pi}}\sigma(\sigma+1)\tau^{3/2}}{9(\sigma+\tau)^{5/2}}, \quad (\text{A4e})$$

$$\mathcal{C}_{ab20}^{SF01} = -\frac{16v_{ab}\sqrt{\frac{2}{\pi}}\sigma(\sigma+1)\tau^{3/2}}{9(\sigma+\tau)^{5/2}}, \quad (\text{A4f})$$

$$\mathcal{C}_{ab01}^{SF01} = \frac{32v_{ab}\sigma(\sigma+1)\tau^{3/2}}{9\sqrt{\pi}(\sigma+\tau)^{5/2}}, \quad (\text{A4g})$$

$$\mathcal{C}_{ab10}^{SF30} = -\frac{4v_{ab}\sqrt{\frac{6}{\pi}}\sqrt{\sigma(\sigma+1)\tau^3}}{5(\sigma+\tau)^2}, \quad (\text{A4h})$$

$$\mathcal{C}_{ab30}^{SF30} = \frac{36v_{ab}(\sigma\tau)^{3/2}}{25\sqrt{\pi}(\sigma+\tau)^{5/2}}, \quad (\text{A4i})$$

$$\mathcal{C}_{ab11}^{SF30} = -\frac{12v_{ab}\sqrt{\frac{6}{\pi}}(\sigma\tau)^{3/2}}{25(\sigma+\tau)^{5/2}}, \quad (\text{A4j})$$

$$\mathcal{C}_{ab10}^{SF11} = \frac{8v_{ab}\sqrt{\sigma(\sigma+1)\tau^3}}{5\sqrt{\pi}(\sigma+\tau)^2}, \quad (\text{A4k})$$

$$\mathcal{C}_{ab30}^{SF11} = -\frac{12v_{ab}\sqrt{\frac{6}{\pi}}(\sigma\tau)^{3/2}}{25(\sigma+\tau)^{5/2}}, \quad (\text{A4l})$$

$$\mathcal{C}_{ab11}^{SF11} = \frac{24v_{ab}(\sigma\tau)^{3/2}}{25\sqrt{\pi}(\sigma+\tau)^{5/2}}. \quad (\text{A4m})$$

for the test and field components, respectively. Finally and for completeness, we report the non-vanishing coefficients of the DK Coulomb collision operator of the test \mathcal{C}_{ab}^{LT} and the field \mathcal{C}_{ab}^{LF} components respectively, i.e.

$$\mathcal{C}_{ab10}^{LT10} = -\frac{8v_{ab}(\sigma+1)}{3\sqrt{\pi}} \left(\frac{\tau}{\sigma+\tau} \right)^{3/2}, \quad (\text{A5a})$$

$$\mathcal{C}_{ab30}^{LT10} = \frac{4}{5} \sqrt{\frac{6}{\pi}} (\sigma+1) \left(\frac{\tau}{\sigma+\tau} \right)^{5/2}, \quad (\text{A5b})$$

$$\mathcal{C}_{ab11}^{LT10} = -\frac{8v_{ab}(\sigma+1)}{5\sqrt{\pi} \left(\frac{\tau}{\sigma+\tau} \right)^{5/2}}, \quad (\text{A5c})$$

$$\mathcal{C}_{ab00}^{LT20} = -\frac{8v_{ab}\sqrt{\frac{2}{\pi}}(\tau-1)\sqrt{\frac{\tau}{\sigma}}}{3\left(\frac{\sigma+\tau}{\sigma}\right)^{3/2}}, \quad (\text{A5d})$$

$$\mathcal{C}_{ab20}^{LT20} = -\frac{v_{ab}8\left(\frac{\tau}{\sigma}\right)^{3/2}(\sigma(10\sigma+\tau+13)+4\tau)}{15\sqrt{\pi}\sigma\left(\frac{\sigma+\tau}{\sigma}\right)^{5/2}}, \quad (\text{A5e})$$

$$\mathcal{C}_{ab01}^{LT20} = \frac{8v_{ab}\sqrt{\frac{2}{\pi}}\left(\frac{\tau}{\sigma}\right)^{3/2}(-3\sigma\tau+\sigma-2\tau)}{15\sigma\left(\frac{\sigma+\tau}{\sigma}\right)^{5/2}}, \quad (\text{A5f})$$

$$\mathcal{C}_{ab00}^{LT01} = \frac{16v_{ab}(\tau-1)\sqrt{\frac{\tau}{\sigma}}}{3\sqrt{\pi}\left(\frac{\sigma+\tau}{\sigma}\right)^{3/2}}, \quad (\text{A5g})$$

$$\mathcal{C}_{ab20}^{LT01} = \frac{8\sqrt{\frac{2}{\pi}}\left(\frac{\tau}{\sigma}\right)^{3/2}(-3\sigma\tau+\sigma-2\tau)}{15\sigma\left(\frac{\sigma+\tau}{\sigma}\right)^{5/2}}, \quad (\text{A5h})$$

$$\mathcal{C}_{ab01}^{LT01} = -\frac{16\left(\frac{\tau}{\sigma}\right)^{3/2}(\sigma(5\sigma-\tau+7)+\tau)}{15\sqrt{\pi}\sigma\left(\frac{\sigma+\tau}{\sigma}\right)^{5/2}}, \quad (\text{A5i})$$

$$\mathcal{C}_{ab10}^{LT30} = -\frac{4v_{ab}}{5\sigma^2}\sqrt{\frac{2}{3\pi}}\sqrt{\frac{\tau}{\sigma}}\left(\frac{\sigma}{\sigma+\tau}\right)^{5/2}(10\sigma^2(\tau-1)+\sigma(\tau-4)\tau-3\tau^2), \quad (\text{A5j})$$

$$\mathcal{C}_{ab30}^{LT30} = -\frac{4v_{ab}\left(\frac{\tau}{\sigma+\tau}\right)^{3/2}(14\sigma^2(\tau+8)+70\sigma^3+\sigma\tau(19\tau+68)+31\tau^2)}{35\sqrt{\pi}(\sigma+\tau)^2}, \quad (\text{A5k})$$

$$\mathcal{C}_{ab11}^{LT30} = \frac{4v_{ab}\sqrt{\frac{2}{3\pi}}\left(\frac{\tau}{\sigma+\tau}\right)^{3/2}(\sigma^2(14-42\tau)+\sigma\tau(3\tau-32)-\tau^2)}{35(\sigma+\tau)^2}, \quad (\text{A5l})$$

$$\mathcal{C}_{ab10}^{LT11} = \frac{8v_{ab}\sqrt{\frac{\tau}{\sigma}}(10\sigma^2(\tau-1)+\sigma(\tau-4)\tau-3\tau^2)}{15\sqrt{\pi}\sigma^2\left(\frac{\sigma+\tau}{\sigma}\right)^{5/2}}, \quad (\text{A5m})$$

$$\mathcal{C}_{ab30}^{LT11} = \frac{4v_{ab}\sqrt{\frac{2}{3\pi}}\left(\frac{\tau}{\sigma+\tau}\right)^{3/2}(\sigma^2(14-42\tau)+\sigma\tau(3\tau-32)-\tau^2)}{35(\sigma+\tau)^2}, \quad (\text{A5n})$$

$$\mathcal{C}_{ab11}^{LT11} = -\frac{8v_{ab}\left(\frac{\tau}{\sigma+\tau}\right)^{3/2}(7(15\sigma+23)\sigma^2+(27\sigma+47)\tau^2+2(21\sigma+59)\sigma\tau)}{105\sqrt{\pi}(\sigma+\tau)^2}, \quad (\text{A5o})$$

and

$$\mathcal{C}_{ab10}^{LF10} = \frac{8v_{ab}(\sigma+1)\tau}{3\sqrt{\pi}\sigma} \left(\frac{\sigma}{\sigma+\tau} \right)^{3/2}, \quad (\text{A6a})$$

$$\mathcal{C}_{ab30}^{LF10} = -\frac{4v_{ab}\sqrt{\frac{6}{\pi}}(\sigma+1)\tau}{5\sigma} \left(\frac{\sigma}{\sigma+\tau} \right)^{5/2}, \quad (\text{A6b})$$

$$\mathcal{C}_{ab11}^{LF10} = \frac{8v_{ab}(\sigma+1)\tau}{5\sqrt{\pi}\sigma} \left(\frac{\sigma}{\sigma+\tau} \right)^{5/2}, \quad (\text{A6c})$$

$$\mathcal{C}_{ab00}^{LF20} = -\frac{8v_{ab}\sqrt{\frac{2}{\pi}}(\tau-1)\sqrt{\frac{\tau}{\sigma}}}{3\left(\frac{\sigma+\tau}{\sigma}\right)^{3/2}}, \quad (\text{A6d})$$

$$\mathcal{C}_{ab20}^{LF20} = \frac{8v_{ab}\sqrt{\frac{\tau}{\sigma}}(\sigma(3\tau-1)+2\tau)}{5\sqrt{\pi}\sigma\left(\frac{\sigma+\tau}{\sigma}\right)^{5/2}}, \quad (\text{A6e})$$

$$\mathcal{C}_{ab01}^{LF20} = \frac{8v_{ab}\sqrt{\frac{2}{\pi}}\sqrt{\frac{\tau}{\sigma}}(-3\sigma\tau+\sigma-2\tau)}{15\sigma\left(\frac{\sigma+\tau}{\sigma}\right)^{5/2}}, \quad (\text{A6f})$$

$$\mathcal{C}_{ab00}^{LF01} = \frac{16(\tau-1)\sqrt{\frac{\tau}{\sigma}}}{3\sqrt{\pi}\left(\frac{\sigma+\tau}{\sigma}\right)^{3/2}}, \quad (\text{A6g})$$

$$\mathcal{C}_{ab20}^{LF01} = \frac{8\sqrt{\frac{2}{\pi}}\sqrt{\frac{\tau}{\sigma}}(-3\sigma\tau+\sigma-2\tau)}{15\sigma\left(\frac{\sigma+\tau}{\sigma}\right)^{5/2}}, \quad (\text{A6h})$$

$$\mathcal{C}_{ab01}^{LF01} = \frac{32\sqrt{\frac{\tau}{\sigma}}(\sigma(3\tau-1)+2\tau)}{15\sqrt{\pi}\sigma\left(\frac{\sigma+\tau}{\sigma}\right)^{5/2}}, \quad (\text{A6i})$$

$$\mathcal{C}_{ab10}^{LF30} = -\frac{4v_{ab}\sqrt{\frac{6}{\pi}}\tau(\sigma(3\tau-2)+\tau)}{5\sigma^2\left(\frac{\sigma+\tau}{\sigma}\right)^{5/2}}, \quad (\text{A6j})$$

$$\mathcal{C}_{ab30}^{LF30} = \frac{12v_{ab}\tau(\sigma(5\tau-2)+3\tau)}{7\sqrt{\pi}(\sigma+\tau)^2\left(\frac{\sigma+\tau}{\sigma}\right)^{3/2}}, \quad (\text{A6k})$$

$$\mathcal{C}_{ab11}^{LF30} = -\frac{12v_{ab}\sqrt{\frac{6}{\pi}}\tau(\sigma(5\tau-2)+3\tau)}{35(\sigma+\tau)^2\left(\frac{\sigma+\tau}{\sigma}\right)^{3/2}}, \quad (\text{A6l})$$

$$\mathcal{C}_{ab10}^{LF11} = \frac{8v_{ab}\tau(\sigma(3\tau-2)+\tau)}{5\sqrt{\pi}\sigma^2\left(\frac{\sigma+\tau}{\sigma}\right)^{5/2}}, \quad (\text{A6m})$$

$$\mathcal{C}_{ab30}^{LF11} = -\frac{12v_{ab}\sqrt{\frac{6}{\pi}}\tau(\sigma(5\tau-2)+3\tau)}{35(\sigma+\tau)^2\left(\frac{\sigma+\tau}{\sigma}\right)^{3/2}}, \quad (\text{A6n})$$

$$\mathcal{C}_{ab11}^{LF11} = \frac{48v_{ab}\tau(\sigma(5\tau-2)+3\tau)}{35\sqrt{\pi}(\sigma+\tau)^2\left(\frac{\sigma+\tau}{\sigma}\right)^{3/2}}, \quad (\text{A6o})$$

respectively. The lowest-order gyro-moments of the IS, OS and Coulomb reported above can be used to obtain reduced-fluid models to study the plasma dynamics in the Pfirsch-Schlüter regime.

REFERENCES

- ¹E. A. Belli and J. Candy, “Implications of advanced collision operators for gyrokinetic simulation,” *Plasma Physics and Controlled Fusion* **59**, 045005 (2017).
- ²M. Barnes, I. G. Abel, W. Dorland, D. R. Ernst, G. W. Hammett, P. Ricci, B. N. Rogers, A. A. Schekochihin, and T. Tatsuno, “Linearized model Fokker–Planck collision operators for gyrokinetic simulations. ii. numerical implementation and tests,” *Physics of Plasmas* **16**, 072107 (2009).
- ³P. Manas, Y. Camenen, S. Benkadda, W. A. Hornsby, and A. G. Peeters, “Enhanced stabilisation of trapped electron modes by collisional energy scattering in tokamaks,” *Physics of Plasmas* **22**, 062302 (2015).
- ⁴Q. Pan, D. R. Ernst, and P. Crandall, “First implementation of gyrokinetic exact linearized Landau collision operator and comparison with models,” *Physics of Plasmas* **27**, 042307 (2020).
- ⁵B. J. Frei, J. Ball, A. C. D. Hoffmann, R. Jorge, P. Ricci, and L. Stenger, “Development of advanced linearized gyrokinetic collision operators using a moment approach,” *Journal of Plasma Physics* **87**, 905870501 (2021).
- ⁶E. A. Belli and J. Candy, “Full linearized fokker–planck collisions in neoclassical transport simulations,” *Plasma physics and controlled fusion* **54**, 015015 (2011).
- ⁷M. N. Rosenbluth, W. M. MacDonald, and D. L. Judd, “Fokker-Planck equation for an inverse-square force,” *Physical Review* **107**, 1 (1957).
- ⁸J. P. Dougherty, “Model Fokker-Planck equation for a plasma and its solution,” *The Physics of Fluids* **7**, 1788 (1964).
- ⁹S. P. Hirshman and D. J. Sigmar, “Approximate Fokker-Planck collision operator for transport theory applications,” *The Physics of Fluids* **19**, 1532 (1976).
- ¹⁰I. G. Abel, M. Barnes, S. C. Cowley, W. Dorland, and A. A. Schekochihin, “Linearized model Fokker-Planck collision operators for gyrokinetic simulations. i. theory,” *Physics of Plasmas* **15**, 122509 (2008).
- ¹¹M. Francisquez, J. Juno, A. Hakim, G. W. Hammett, and D. R. Ernst, “Improved multispecies

Implementation of the Improved Sugama Collision Operator

- dougherty collisions,” arXiv preprint arXiv:2109.10381 (2021).
- ¹²H. Sugama, T.-H. Watanabe, and M. Nunami, “Linearized model collision operators for multiple ion species plasmas and gyrokinetic entropy balance equations,” Physics of Plasmas **16**, 112503 (2009).
- ¹³M. Nunami, M. Nakata, T.-H. Watanabe, and H. Sugama, “Development of linearized collision operator for multiple ion species in gyrokinetic flux-tube simulations,” Plasma and Fusion Research **10**, 1403058 (2015).
- ¹⁴M. Nakata, M. Nunami, T.-H. Watanabe, and H. Sugama, “Improved collision operator for plasma kinetic simulations with multi-species ions and electrons,” Computer Physics Communications **197**, 61 (2015).
- ¹⁵Q. Pan, D. R. Ernst, and D. R. Hatch., “Importance of gyrokinetic exact Fokker-Planck collisions in fusion plasma turbulence,” Physical Review E **103**, L051202 (2021).
- ¹⁶B. J. Frei, A. C. D. Hoffmann, and P. Ricci, “Local gyrokinetic collisional theory of the ion-temperature gradient mode,” arXiv preprint arXiv:2201.02860 (2022).
- ¹⁷H. Sugama, S. Matsuoka, S. Satake, M. Nunami, and T.-H. Watanabe, “Improved linearized model collision operator for the highly collisional regime,” Physics of Plasmas **26**, 102108 (2019).
- ¹⁸S. P. Hirshman and D. J. Sigmar, “Neoclassical transport of impurities in tokamak plasmas,” Nuclear Fusion **21**, 1079 (1981).
- ¹⁹M. Honda, “Impact of higher-order flows in the moment equations on pfirsch-schlüter friction coefficients,” Physics of Plasmas **21**, 092508 (2014).
- ²⁰S. Matsuoka, H. Sugama, and Y. Idomura, “Neoclassical transport simulations with an improved model collision operator,” Physics of Plasmas **28**, 064501 (2021).
- ²¹B. J. Frei, R. Jorge, and P. Ricci, “A gyrokinetic model for the plasma periphery of tokamak devices,” Journal of Plasma Physics **86**, 905860205 (2020).
- ²²R. Jorge, B. J. Frei, and P. Ricci, “Nonlinear gyrokinetic coulomb collision operator,” Journal of Plasma Physics **85**, 905850604 (2019).
- ²³F. Jenko, W. Dorland, M. Kotschenreuther, and B. N. Rogers, “Electron temperature gradient driven turbulence,” Physics of plasmas **7**, 1904 (2000).
- ²⁴F. J. Casson, C. Angioni, E. A. Belli, R. Bilato, P. Mantica, T. Odstrcil, T. Pütterich, M. Valisa, L. Garzotti, C. Giroud, *et al.*, “Theoretical description of heavy impurity transport and its application to the modelling of tungsten in jet and asdex upgrade,” Plasma Physics and Controlled

Implementation of the Improved Sugama Collision Operator

- Fusion **57**, 014031 (2014).
- ²⁵P. Helander and D. J. Sigmar, *Collisional transport in magnetized plasmas*, Vol. 4 (Cambridge University Press, 2005).
- ²⁶R. F. Snider, *Irreducible Cartesian Tensors*, De Gruyter Studies in Mathematical Physics No. 1 (De Gruyter, 2017).
- ²⁷A. J. Brizard and T. Hahm, “Foundations of nonlinear gyrokinetic theory,” Reviews of modern physics **79**, 421 (2007).
- ²⁸P. Crandall, D. Jarema, H. Doerk, Q. Pan, G. Merlo, T. Görler, A. B. Navarro, D. Told, M. Maurer, and F. Jenko, “Multi-species collisions for delta-f gyrokinetic simulations: Implementation and verification with gene,” Computer Physics Communications **255**, 107360 (2020).
- ²⁹R. Jorge, P. Ricci, and N. F. Loureiro, “A drift-kinetic analytical model for scrape-off layer plasma dynamics at arbitrary collisionality,” Journal of Plasma Physics **83**, 905830606 (2017).
- ³⁰I. S. Gradshteyn and I. M. Ryzhik, *Table of integrals, series, and products* (Academic press, 2014).
- ³¹D. P. Fulton, Z. Lin, I. Holod, and Y. Xiao, “Microturbulence in dIII-D tokamak pedestal. i. electrostatic instabilities,” Physics of Plasmas **21**, 042110 (2014).
- ³²M. Kotschenreuther, D. R. Hatch, S. Mahajan, P. Valanju, L. Zheng, and X. Liu, “Pedestal transport in h-mode plasmas for fusion gain,” Nuclear Fusion **57**, 064001 (2017).
- ³³M. J. Pueschel, D. R. Hatch, D. R. Ernst, W. Guttenfelder, P. W. Terry, J. Citrin, and J. W. Connor, “On microinstabilities and turbulence in steep-gradient regions of fusion devices,” Plasma Physics and Controlled Fusion **61**, 034002 (2019).
- ³⁴H.-S. Xie and B. Li, “Global theory to understand toroidal drift waves in steep gradient,” Physics of Plasmas **23**, 082513 (2016).
- ³⁵M. Han, Z.-X. Wang, J. Dong, and H. Du, “Multiple ion temperature gradient driven modes in transport barriers,” Nuclear Fusion **57**, 046019 (2017).
- ³⁶D. M. Thomas, A. W. Leonard, T. H. Osborne, R. J. Groebner, W. P. West, and K. H. Burrell, “The effect of plasma collisionality on pedestal current density formation in DIII-D,” Plasma physics and controlled fusion **48**, A183 (2006).
- ³⁷X. Lapillonne, S. Brunner, T. Dannert, S. Jolliet, A. Marinoni, L. Villard, T. Görler, F. Jenko, and F. Merz, “Clarifications to the limitations of the s- α equilibrium model for gyrokinetic computations of turbulence,” Physics of Plasmas **16**, 032308 (2009).
- ³⁸J. W. Connor, R. J. Hastie, and P. Helander, “Stability of the trapped electron mode in steep

Implementation of the Improved Sugama Collision Operator

- density and temperature gradients,” *Plasma physics and controlled fusion* **48**, 885 (2006).
- ³⁹M. N. Rosenbluth and F. L. Hinton, “Poloidal flow driven by ion-temperature-gradient turbulence in tokamaks,” *Physical Review Letters* **80**, 724 (1998).
- ⁴⁰P. H. Diamond, S. I. Itoh, K. Itoh, and T. S. Hahm, “Zonal flows in plasma—a review,” *Plasma Physics and Controlled Fusion* **47**, R35 (2005).
- ⁴¹F. L. Hinton and M. N. Rosenbluth, “Dynamics of axisymmetric ($E \times B$) and poloidal flows in tokamaks,” *Plasma Physics and Controlled Fusion* **41**, A653 (1999).
- ⁴²Y. Xiao, P. J. Catto, and K. Molvig, “Collisional damping for ion temperature gradient mode driven zonal flow,” *Physics of Plasmas* **14**, 032302 (2007).